HHS Public Access

Author manuscript

Neuron. Author manuscript; available in PMC 2016 May 06.

Published in final edited form as:

Neuron. 2015 May 6; 86(3): 680–695. doi:10.1016/j.neuron.2015.04.003.

Molecular substrates of altered axonal growth and brain connectivity in a mouse model of schizophrenia

Jun Mukai[1], **Makoto Tamura**[2,3], **Karine Fénelon**[1,6], **Andrew M. Rosen**[1,2], **Timothy J. Spellman**[1], **Rujun Kang**[4], **Amy B. MacDermott**[1,5], **Maria Karayiorgou**[2], **Joshua A. Gordon**[2], and **Joseph A. Gogos**[1,5,*]

[1]Department of Physiology and Cellular Biophysics, College of Physicians and Surgeons, Columbia University, New York, New York 10032 USA

[2]Department of Psychiatry, New York State Psychiatry Institute, New York, New York 10032 USA

[3]Pharmacology Research Laboratories I, Mitsubishi Tanabe Pharma Corporation. Yokohama, Kanagawa 227-0033 Japan

[4]Department of Psychiatry, University of British Columbia, Vancouver, British Columbia, V6T 1Z3 Canada

[5]Department of Neuroscience, College of Physicians and Surgeons, Columbia University, New York, New York 10032 USA

Summary

22q11.2 deletion carriers show specific cognitive deficits and ~30% of them develop schizophrenia. One of the disrupted genes is *ZDHHC8*, which encodes for a palmitoyltransferase. We show that *Zdhhc8*-deficient mice have reduced palmitoylation of proteins that regulate axonal growth and branching. Analysis of axonal projections of pyramidal neurons from both *Zdhhc8*-deficient and *Df(16)A*$^{+/-}$ mice, which model the 22q11.2 deletion, revealed deficits in axonal growth and terminal arborization, which can be prevented by reintroduction of active ZDHHC8 protein. Impaired terminal arborization is accompanied by a reduction in the strength of synaptic connections and altered functional connectivity and working memory. The effect of ZDHHC8 is mediated in part via Cdc42-dependent modulation of Akt/Gsk3β signaling at the tip of the axon and can be reversed by pharmacologically decreasing Gsk3β activity during postnatal brain development. Our findings provide valuable mechanistic insights into the cognitive and psychiatric symptoms associated with a schizophrenia-predisposing mutation.

*Correspondence: jag90@columbia.edu (J.A.G).

[6]Present address: Department of Biological Sciences, Bioscience Research Building, University of Texas at El Paso, El Paso, TX, 79968 USA

Mukai et al. found that a mutation that predisposes to schizophrenia affects proteins involved in axonal growth leading to alterations in axonal connectivity and the function of local and long-range neural circuits. Early pharmacological intervention can restore these deficits.

INTRODUCTION

Deletions of the 22q11.2 locus are among the most common chromosomal abnormalities and occur predominantly de novo (McDonald-McGinn et al., 2001). Children with the 22q11.2 deletion show a spectrum of cognitive deficits (Woodin et al., 2001; Bearden et al., 2001), a high incidence of emotional problems (Woodin et al., 2001) in childhood and ∼30% of them develop schizophrenia in adolescence or early adulthood (Pulver et al., 1994). New 22q11.2 deletions account for 1–2% of sporadic schizophrenia cases (Xu et al., 2008). Most affected individuals carry a 3-Mb deletion, whereas 7% have a nested 1.5-Mb deletion spanning 27 known genes

Previous work has provided insights into the genetic basis of the psychiatric and cognitive symptoms observed in carriers of 22q11.2 deletions and implicated a subset of these genes including *ZDHHC8* (Mukai et al., 2004). Notably, a genetic variant of *ZDHHC8* that modulates the complex splicing pattern at this locus was associated with schizophrenia in some cohorts of karyotypically normal patients (Mukai et al., 2004; Chen et al., 2004). *ZDHHC8* is a palmitoyltransferase belonging to a 23-member family of enzymes that share a conserved cysteine-rich signature catalytic domain (DHHC domain) (Fukata et al., 2010). Protein palmitoylation describes the addition of the saturated 16-carbon palmitate lipid at specific cysteine residues by a liable thioester bond (el-Husseini and Bredt, 2002) and has emerged as a key reversible post-translational protein modification involved in the protein trafficking and the regulation of diverse membrane and cytosolic proteins, especially in neurons (el-Husseini and Bredt, 2002)._The biochemical machinery involved has only recently been identified and our earlier work established a connection between palmitoylation and neural signaling *in vivo* (Mukai et al. 2008).

Using chromosomal engineering, we generated the *Df(16)A*$^{+/-}$ mouse model, which carries a 1.3-Mb chromosomal deficiency (*Df(16)A*) that is syntenic to the human 22q11.2 1.5-Mb deletion (Stark et al., 2008). We also reported the generation and characterization of a mouse strain carrying a deletion of the *Zdhhc8* gene (Mukai et al., 2004; Mukai et al., 2008). We have previously shown that *Df(16)A*$^{+/-}$ mice have reduced dendritic branching and spine density in hippocampal neurons, a phenotype, which is also observed in *Zdhhc8*-deficient mice (Mukai et al., 2008). We also provided evidence that PSD95, a key postsynaptic protein, is one of the substrates of ZDHHC8, a finding replicated recently by Ho et al. (2011) and Yoshii et al. (2011).

As part of our systematic efforts to identify additional ZDHHC8 substrates, we made the unexpected discovery that *Zdhhc8* deficiency affects palmitoylation of a number of proteins thought to regulate axonal growth and branching. By following up this finding, we present the results of a comprehensive analysis of axonal projections of pyramidal neurons from both *Df(16)A*$^{+/-}$ and *Zdhhc8*-deficient mice. We found that mutant mice have deficits in axonal growth during embryogenesis as well as in terminal arborization, which can be prevented by reintroduction of enzymatically active ZDHHC8. Impaired terminal arborization of pyramidal neurons is accompanied by a reduction in the strength of synaptic connections as well as altered functional connectivity and spatial working memory (WM) performance. Finally, using genetic and pharmacological rescue, we show that the effect of

ZDHHC8 on axon growth is mediated in part via Cdc42-dependent modulation of Akt/Gsk3β signaling at the tip of the axon. The palmitoylation-dependent changes in structural connectivity we describe represent possible predisposing factors to the psychiatric and cognitive symptoms associated with the 22q11.2 deletion.

RESULTS

Palmitoyl-proteome in *Zdhhc8*-deficient neurons

To find substrates of ZDHHC8 palmitoyltransferase activity we employed the acyl-biotinyl exchange (ABE) proteomic technology (Wan et al., 2007), which purifies palmitoylated proteins from complex protein extracts. Proteins extracted from cultured mouse embryonic cortical neurons from *Zdhhc8*$^{-/-}$ and wild-type (WT) mice at DIV21 were used for this analysis.

We have previously shown that PSD95 is a ZDHHC8 substrate (Mukai et al., 2008; Ho et al., 2011). Other proposed ZDHHC8 substrates include GAP43 (Mukai et al., 2008) and GRIP1 (Thomas et al., 2012). ABE analysis showed that, compared with WT neurons, palmitoylation level of PSD-95 was reduced by 30% in *Zdhhc8*$^{-/-}$ (*Zdhhc8*$^{-/-}$: 22 mice, n = 22; *Zdhhc8*$^{+/+}$: 21 mice, n = 21, $P < 0.0003$), (Figure 1A). GRIP1 was also reduced 26% in *Zdhhc8*$^{-/-}$ (*Zdhhc8*$^{-/-}$: 17 mice, n = 17; *Zdhhc8*$^{+/+}$: 16 mice, n = 16, $P < 0.005$) (Figures 1A and 1B). Palmitoylation of GAP43 was reduced by 17% in *Zdhhc8*$^{-/-}$ neurons (*Zdhhc8*$^{-/-}$: 26 mice, n = 26; *Zdhhc8*$^{+/+}$: 28 mice, n = 28, $P < 0.001$). In contrast, SNAP25 (*Zdhhc8*$^{-/-}$: 112 %, 17 mice, n = 17; *Zdhhc8*$^{+/+}$: 16 mice, n = 16, $P > 0.1$) and Synaptotagmin I (*Zdhhc8*$^{-/-}$: 99 %, 17 mice, n = 17; *Zdhhc8*$^{+/+}$: 16 mice, n = 16, $P > 0.1$), which were not palmitoylated by ZDHHC8 *in vitro* (Mukai et al., 2008), showed no change of palmitoylation level in *Zdhhc8*$^{-/-}$ neurons as assayed by ABE. Having validated our approach we looked for additional substrates.

The strongest reduction of palmitoylation in *Zdhhc8*$^{-/-}$ neurons was observed for Rho GTPases, Cdc42 and Rac1, which regulate actin cytoskeleton and cellular morphology inducing filopodia and lamellipodia in many cell types (Iden et al., 2008), while in neurons they have been implicated in the regulation of axonal development and cell polarity (Tahirovic et al., 2010 ; Garvalov et al., 2007; Nishimura et al., 2005; Schwamborn et al., 2004). In *Zdhhc8*$^{-/-}$ neurons, palmitoylation of Cdc42 was reduced by 33% (*Zdhhc8*$^{-/-}$: 17 mice, n = 17; *Zdhhc8*$^{+/+}$: 16 mice, n = 16, $P < 0.005$) and palmitoylation of Rac1 was reduced by 38% (*Zdhhc8*$^{-/-}$: 17 mice, n = 17; *Zdhhc8*$^{+/+}$: 16 mice, n = 16, $P < 0.0001$).

Zdhhc8 deficiency disrupts axonal growth

Our finding that ZDHHC8 palmitoylates a number of proteins involved in axonal development prompted us to investigate the role of Zdhhc8 in this process. To this end, we first used cortical cultures from *Zdhhc8* deficient mice (*Zdhhc8*$^{+/-}$, *Zdhhc8*$^{-/-}$) and *Zdhhc8*$^{+/+}$ littermates (Figure S1A). Dissociated cortical neurons were cultured for 3 days and axon polarity was analyzed by staining with anti-Tau-1 antibody as an axon specific marker, anti- MAP2 antibody as a dendritic marker, and with phalloidin to visualize the whole neuron. Control WT cortical neurons developed normal polarity, with most of them

having a single axon and multiple dendrites (77. 0 ± 0.9% and 3.4 ± 0.5%, respectively), and 19.6 ± 1.2% of neurons with no discernable axon. *Zdhhc8* deficiency significantly reduced the portion of neurons having a single axon (*Zdhhc8*$^{+/-}$: 67.3 ± 1.3%, $P < 0.0001$; *Zdhhc8*$^{-/-}$, 62.1 ± 1.8%, $P < 0.0001$) (Figure S1A and S1B). The axons of *Zdhhc8*-deficient neurons were also significantly shorter than those of the WT cells (Figure S1C). The length and number of dendrites were modestly, but significantly reduced in *Zdhhc8*-deficient neurons (Figure S1D and S1E).

To elaborate further on this observation, dissociated cortical neurons were transfected with a plasmid for EGFP at DIV2 and cultured for 4 days before analysis of axon length and branching. Primary axon length was reduced in *Zdhhc8*$^{+/-}$ and *Zdhhc8*$^{-/-}$ neurons at DIV4 (341.2 ± 14.6 μm, n = 24, $P < 0.05$; 305.2 ± 22.2 μm, n = 24, $P < 0.005$), compared to *Zdhhc8*$^{+/+}$ neurons (421.4 ± 17.1 μm, n = 24) (Figures 1C and 1D). Specifically, *Zdhhc8* deficiency caused a decrease in the number of branch points in both *Zdhhc8*$^{+/-}$ (4.0 ± 0.3, n = 24, $P < 0.05$) and *Zdhhc8*$^{-/-}$ (3.3 ± 0.3, n = 24, $P < 0.001$) neurons compared to *Zdhhc8*$^{+/+}$ neurons (5.3 ± 0.3, n = 24; Figures 1C and 1D) respectively. To confirm that the effect on axonal growth was directly mediated via ZDHHC8 transferase activity, we expressed the full-length enzymatically active form (ZDHHC8-FL) or an enzymatically inactive form (ZDHHC8-C134A) in cortical neurons from *Zdhhc8*$^{-/-}$ mice. In *Zdhhc8*$^{-/-}$ neurons expressing ZDHHC8-FL (n = 24), the numbers of total branch points (5.2 ± 0.3, n = 24, $P < 0.05$) and primary axon length (397.0 ± 22.7, n = 24, $P < 0.05$) were restored to *Zdhhc8*$^{+/+}$ levels, whereas the enzymatically inactive form (n = 18) did not influence these parameters (Figures 1C and 1D).

Prompted by these findings, we investigated further whether palmitoylation in general regulates axon polarity. The consequence of suppressing palmitoylation in developing neurons was examined using 2-bromopalmitate (2-BP), an inhibitor to palmitoyltransferase activity, to treat cultured cortical neurons during the transition from stage 2 to stage 3, a critical period in which rapid axonal growth and polarization occur (Yoshimura et al., 2006). While most WT cells displayed a single neurite marked by the axonal marker Tau-1 (78.0 ± 0.5 % of the cells), treatment with 2-BP reduced neurons with a single Tau-1 positive neurite (to 56.0 ± 1.1 % of cells treated with 0.1 μM 2-BP) (Figure S1F and S1G). Both axons (Figure S1F and S1H) and MAP2-stained dendrites (Figure S1I and S1J) of treated cells were significantly shorter (in a dosage dependent manner) than that of untreated cells. In addition, analysis of axon branching at DIV4 (following treatment with 0.1 μM 2-BP) revealed a reduction in primary axon length compared to control neurons (288.0 ± 11.2 μm versus 432.5 ± 23.9 μm, n = 18, $P < 0.001$) as well as a significant decrease in the number of branch points compared to control neurons (2.3 ± 0.2 μm versus 5.8 ± 0.5μm, n = 18, $P < 0.005$) (Figure S1M–S1P). Interestingly, 0.1 μM 2-BP treatment further reduced the portion of *Zdhhc8*$^{-/-}$ single axon cells compared to untreated *Zdhhc8*$^{-/-}$ cells (49.8 ± 2.2 % versus 62.0 ± 1.8 %, Figure S1K and S1L), suggesting that other DHHC isoforms might also contribute to modulate neuronal polarity.

ZDHHC8 Activity Is Required for Axon Growth *in Vivo*

To determine the effect of ZDHHC8 activity on axon development *in vivo*, we used *in utero* electroporation to express EGFP in newly divided cortical neurons of *Zdhhc8*$^{-/-}$ embryos and examine axon morphology at a single-cell resolution (Figure S2A). Following electroporation at E14.5, embryos were placed back into the mother and allowed to develop for an additional 3 days (E17.5), at which point the morphology of EGFP-positive migrating neurons was examined. Electroporated neurons in both control and mutant cortices had migrated through the intermediate zone (IZ) and reached the cortical plate (CP) (Figure S2A), indicating that ZDHHC8 is dispensable for proper radial migration.

When neuronal migration through the cortical plate is completed, transfected layers 2/3 neurons show a polarized morphology with developing dendritic arbors and thin, straight axons. In WT brains, EGFP-expressing neurons show a typical basal axon and multiple apical dendrites derived from a single dendritic base (Figure S2B and S2C). The vast majority of both WT and mutant neurons have a single axon. Although we cannot exclude subtle polarity differences among genotypes, *Zdhhc8* deficiency does not appear to have a strong effect on polarity *in vivo*. This likely relates to the redundancy of DHHC palmitoyltransferases and polarity signaling pathways. On the other hand, examination of the length of axons in WT or *Zdhhc8*-deficient cortices confirmed that *Zdhhc8* deficiency resulted in a decrease in axon length [11% in *Zdhhc8*$^{+/-}$ (n = 24, $P < 0.05$), 25% in *Zdhhc8*$^{-/-}$ (n = 24, $P < 0.001$)] compared with *Zdhhc8*$^{+/+}$ brains (n = 24) (Figure S2B and S2C). Expression of ZDHHC8 FL (n = 18) restored axonal length in *Zdhhc8*$^{-/-}$ brains to *Zdhhc8*$^{+/+}$ levels (Figure S2B and S2C).

To investigate further the role of ZDHHC8 on axonal branching, plasmids encoding EGFP were electroporated *in utero* into the dorsolateral ventricular zone of the mouse forebrain at E15.5 and embryos were allowed to be born and develop to P8.5 for analysis. All cells labeled with EGFP completed their migration into layers 2/3 by P8.5. As shown previously (Jeanneteau et al., 2010), callosal axons crossed the midline, coursed beneath the gray matter of the contralateral somatosensory cortex, penetrated the gray matter and ascended to layers 1–3 and 5 (Figure 2A).

The number of callosal axon terminal branches within the contralateral cortical layers 1–4 was decreased by disruption of *Zdhhc8* with notably fewer secondary branches [total branch number: 34% in *Zdhhc8*$^{+/-}$ (n = 19, $P < 0.0001$), 45% in *Zdhhc8*$^{-/-}$ (n = 19, $P < 0.0001$)], compared with *Zdhhc8*$^{+/+}$ brains (n = 19) (Figures 2B, 2D and 2E). Analysis of the collateral branching of axons within the ipsilateral cortical layers 2–4 (Figures 2C and 2F) showed that disruption of *Zdhhc8* resulted in a decrease in the number of axonal branches [23% in *Zdhhc8*$^{+/-}$(n = 19, $P < 0.001$), 31% in *Zdhhc8*$^{-/-}$ (n = 19, $P < 0.0001$)] compared with *Zdhhc8*$^{+/+}$ brains (n = 19) (Figure 2G). To confirm that the effect on axonal branching was directly mediated via ZDHHC8 activity we electroporated a construct driving both EGFP and ZDHHC8FL (*ZDHHC8FL::IRES-EGFP*) into *Zdhhc8*$^{-/-}$ embryos *in utero*. Restricting our analysis to ipsilateral projections we showed that ZDHHC8FL expression reversed the number of axonal branches in cortical layers 2–4 to WT levels (Figures 2H and 2I).

To examine whether reduced axonal arborization persists in adulthood, mice were electroporated with EGFP at E15.5 and were sacrificed at P56 to evaluate adult patterns of axonal branching. As shown previously in P21 brain (Courchet et al., 2013), callosal axons of layers 2/3 pyramidal neurons branch extensively between P8.5 and P56 in contralateral layers 1–3 and layer 5 (Figure S2D and Figure 2J) and ipsilateral layers 2/3 and layer 5 (Figure 2K) while avoiding branching in layer 4 and 6 both contralateral and ipsilateral hemispheres. We analyzed EGFP intensity in ipsilateral and contralateral axon target regions to quantify the complexity of axon branching. *Zdhhc8* deficiencyshowed significantly reduced branching contralaterally in both layer 1 and 2/3 (Figure 2J) as well as ipsilaterally in layer 5 (Figure 2L).

Zdhhc8 deficiency disrupts hippocampal projections to mPFC and WM performance

We have previously shown 22q11.2 deletion lead to abnormal PFC–HPC coupling, similar to the one reported in schizophrenia patients (Sigurdsson et al., 2010). Such long-range connectivity deficits may underlie deficits in cognition and other aspects of the clinical diagnosis. We have also reported an impairment of spatial working memory in *Df(16)+/-* mice, which appears to be due in part to altered functional connectivity between the HPC and mPFC (Sigurdsson et al., 2010). The circuit basis for this deficit maybe complex, involving at least in part anatomical connections affected in terms of axonal extension and branching. We therefore asked whether *Zdhhc8* deficiency disrupts the long-range projection from the HPC to mPFC and affects HPC-mPFC synchrony and WM performance.

Initial analysis of axonal morphogenesis in primary hippocampal neurons collected from *Zdhhc8*-deficient mice and their WT littermates revealed a deficit of polarity as well as a pattern and degree of axonal arbor simplification (Figure S3A-S3I) very similar to those observed in *Zdhhc8*-deficient cortical neurons. Most importantly, deficits observed *in vitro* in neuronal cultures are recapitulated in the developing brains of mutant mice. Following *in utero* electroporation of an EGFP construct to ventral hippocampus (vHPC) at E16.5 (Figure S3J), the morphology of EGFP-positive axons was examined in sagittal brain sections during postnatal development. Labeled ventral field CA1axons in both $Zdhhc8^{+/+}$ and $Zdhhc8^{+/-}$ projected normally to frontal regions of the cerebral cortex, extended rostrally through the lateral septal nucleus in the precommissural fornix and reached the dorsal tenia tecta by P7.5. At P16.5 a subset of fibers at the tenia tecta extended dorsally near the genu of the corpus callosum to the infralimbic area, prelimbic area, and the anterior cingulated area (Figure S3J). At P16.5 the number of axon terminal branches in the layer 5 of prelimbic mPFC was significantly reduced in $Zdhhc8^{+/-}$ mice, with notably fewer secondary branches (Figure S3K and Figures 3A-3C). To examine whether reduced axonal arborization persists in adulthood, we injected an adeno-associated virus (rAAV1/hSynapsin/EGFP) into CA1 in the vHPC at P56 (8 weeks) and mice were sacrificed at P84 (12 weeks) (Figure S3L). Evaluation of patterns of axonal branching in mPFC of *Zdhhc8*-deficient mice showed significantly reduced axon branching in layer 5 of prelimbic mPFC (Figures 3D-3F).

To examine the impact of *Zdhhc8* deficiency on long-range functional connectivity and working memory, $Zdhhc8^{+/-}$ mice and their WT littermates were implanted with recording electrodes aimed at the ventral (vHPC) and dorsal hippocampus (dHPC), as well as the

medial prefrontal cortex (mPFC). Neural activity was then recorded at baseline, and during training and testing in the T-maze delayed non-match to sample test of spatial working memory. Behaviorally, *Zdhhc8*$^{+/-}$ mice took significantly longer than WT mice to reach criterion performance on the T-maze task (Figure 3G). *Zdhhc8*$^{+/-}$ mice also showed lower theta-frequency (4–12Hz) coherence between vHPC and mPFC as well as vHPC and dHPC after acquisition of the task (Figures 3H-3K). Although there was no statistically significant difference in theta coherence during a baseline session before training (Figure 3L), baseline theta coherence between vHPC and mPFC was inversely correlated with days to criterion (Figure 3M). Thus, the observed deficits in anatomical connectivity between vHPC and mPFC, due to *Zdhhc8* deficiency are accompanied by a disruption of functional connectivity between these two areas during behavior, which was narrower than that seen with the complete mutation (*Df16(A)*$^{+/-}$ mice; Sigurdsson et al., 2010). In turn, disruption of the long-range projections from HPC to mPFC may contribute, possibly along with more localized deficits in pyramidal and inhibitory neuron function, to the impaired WM performance.

Disrupted axonal growth and branching in *Df(16)A*$^{+/-}$ mice

In addition to the impaired connectivity between vHPC and mPFC, several other salient features identified by our analysis of *Zdhhc8*-deficient mice were recapitulated in *Df(16)A*$^{+/-}$ mice.

First, ABE analysis showed that, compared with WT neurons, palmitoylation level of PSD-95, Cdc42, and Rac1 were reduced in *Df(16)A*$^{+/-}$ (Figure S4A and S4B), but to a lesser extent than in *Zdhhc8*$^{-/-}$ (Figure 1A and 1B).

Second, analysis of axonal morphogenesis in primary cortical neurons from *Df(16)A*$^{+/-}$mice and their WT littermates revealed a pattern and degree of axonal arbor simplification very similar to those observed in *Zdhhc8* deficient neurons.. Specifically, compared to DIV3 WT neurons, *Df(16)A*$^{+/-}$ neurons demonstrated significantly reduced portion of single axon cells (66.0 ± 1.0 % versus 78.0 ± 1.0 % in WT, $P < 0.0001$; Figure S4C and S4D). Also, the axons of *Df(16)A*$^{+/-}$ neurons were significantly shorter than those of the WT cells (78.1 ± 3.0 μm versus 116.2 ± 3.0 μm in WT, $P < 0.0001$; Figure S4E). The length and number of dendrites were also significantly reduced in *Df(16)A*$^{+/-}$ neurons (Figure S4F and S4G) at DIV3.

At DIV4, when axon branching ensues, primary axon length was reduced in *Df(16)A*$^{+/-}$ neurons compared to WT neurons (323.3 ± 13.0 μm versus 409.3 ± 23.7 μm, n = 24, $P < 0.05$; Figure S4H and S4I) and there was a decrease in the number of branch points compared to WT neurons (4.16 ± 0.2 versus 5.6 ± 0.5, n = 24, $P < 0.05$; Figure S4H and S4J). Introduction of ZDHHC8 FL confirmed that the reduction in axonal complexity was a direct effect of reduced Zdhhc8 activity (Figure S4H–S4K).

Deficits observed *in vitro* in neuronal cultures are recapitulated in the developing brain of *Df(16)A*$^{+/-}$ mice, where again the pattern and degree of axonal arbor simplification were very similar to those observed in *Zdhhc8*-deficient mice. Following *in utero* electroporation of an EGFP construct at E14.5, *Df(16)A*$^{+/-}$ embryos were placed back into the mother and

allowed to develop for an additional 3 days (E17.5). Electroporated neurons in both WT and *Df(16)A*$^{+/-}$ had normally migrated through the IZ and reached the CP (Figure S4L). Presence of *Df(16)A* resulted in a 20% decrease in length of axon, located in layers 2/3 (n = 31, $P < 0.0001$), compared with WT (n = 24) (Figure S4M and S4N). *Df(16)A* also resulted in decrease in both ipsi-and contra-lateral axonal branching at P8.5 (Figures 4A–4F). Introduction of ZDHHC8 FL restored axon length (Figure S4M and S4N), and axon branching (Figures 4G and 4H) in *Df(16)A*$^{+/-}$ brain to WT levels. By contrast, introduction of PRODH, one of the deleted genes resting within *Df(16)A* that has a well-defined function not related to protein palmitoylation, did not influence these parameters.

To examine whether reduced axonal arborization persists in adulthood, *Df(16)A*$^{+/-}$ mice were electroporated with EGFP at E15.5 and were sacrificed at P56 to evaluate adult patterns of axonal branching. *Df(16)A*$^{+/-}$ showed significantly reduced branching contralaterally both in layer 1 and 2/3 (Figure 5A) and ipsilaterally in layer 5 (Figures 5B and 5C). To assess whether a decrease in axonal branching of layer 2 pyramidal neurons was associated with a deficit in synaptic efficacy in L2-L5 neurons, we employed an optogenetic approach, in which a vector driving ChR2-Venus together with mCherry was delivered to L2 neurons by *in utero* electroporation at E16.5 (Figure 5D). Using acute coronal brain slices prepared from the frontal cortex of 8-week-old mice, we then performed extracellular recordings ipsilateral to the electroporated hemisphere (Figure 5E). Optical stimulation of the fibers and terminals of the transfected L2 neurons (expressing ChR2) triggered neurotransmitter release recorded as field EPSPs (fEPSPs) in L5 (Figures 5E and 5F). At higher stimulation intensities, the optically evoked fEPSPs were smaller in the *Df(16)A*$^{+/-}$ mice (N = 5, n = 11) compared to their WT littermates (N = 7, n= 16)(Figure 5G, stimulation intensities 3–10, $P < 0.05$). To rule out the possibility that the observed difference in the input-output curve between genotypes could be due to different ChR2 expression in the activated axons, the input-output curves were normalized, and their similitude suggests that ChR2 levels were comparable in each group of activated axons (Figure S5A, $P > 0.05$). It is known that the size of evoked fEPSPs depends on the number of synapses and on the probability of neurotransmitter release. In addition, the probability of vesicular release has been shown to be inversely proportional to the ratio of fEPSPs obtained using paired-pulse stimulation. Therefore, we performed paired-pulse stimulation to determine whether the differences in synaptic strength at higher stimulation intensities were due to differences in the probability of neurotransmitter release at the layers 2–5 synapses between genotypes. Light-evoked PPR was normal in *Df(16)A*$^{+/-}$ mice at a variety of interstimulus intervals (Figure S5B, two-way repeated-measures ANOVA; $P > 0.05$), suggesting that the different fEPSPs amplitudes reflect differences in the number of functional synapses probably due to the decrease in axonal branching of layer 2 pyramidal neurons of *Df(16)A*$^{+/-}$ mice.

Signaling pathways as downstream effectors of ZDHHC8 in mediating axonal growth

Several of the ZDHHC8 substrates represent downstream effectors that could mediate the biological activity of ZDHHC8 on axon growth and branching. We focused on the reduction of palmitoylated Cdc42 in *Zdhhc8*-deficient neurons (Figure 1) given the well-established role of Cdc42 in axonal development and the fact that alterations in Cdc42 expression have

been consistently reported in the brains of patients with psychiatric disorders, including schizophrenia (Gilks et al., 2012; Ide et al., 2010). Genetic ablation of Cdc42 leads to deficits in neuronal polarity and elongation of axons in cultured hippocampal neurons as well as in cortical neurons *in vivo* (Garvalov et al., 2007; Nishimura et al., 2005; Schwamborn et al., 2004), suggesting that Cdc42 may contribute to the axonal phenotypes emerging as a result of the *Zdhhc8* deficiency. Alternative splicing gives rise to two different Cdc42 isoforms: a ubiquitously expressed canonical form (isoform 1) and a brain-specific form (isoform 2: Cdc42Palm) (Nishimura et al., 2013). Canonical Cdc42 carries a CaaX motif (prenylation) at its C-terminal (CVLL), whereas Cdc42Palm carries a double-cysteine CCaX (CCIF) motif. Cdc42Palm is palmitoylated, whereas the canonical form is not (Nishimura et al., 2013; Kang et al., 2008). Wirth et al. (2013) reported that the expression level of Cdc42Palm in the hippocampus was approximately 2-fold higher than that of isoform 1. We specifically examined the involvement of Cdc42Palm in axonal growth.

Exogenous Cdc42Palm fused to EGFP (EGFP- CDC42Palm) is enriched at the axon tip at DIV3 (Figure S6A) whereas a mutant form with disrupted palmitoylation sites (EGFP-C2S) is diffusely localized in the entire cell (Figure S6A). A specific antibody against Cdc42Palm showed an enrichment of the endogenous Cdc42Palm at tip of axon (Figure 6A). 2-BP treatment disrupts this enrichment and diffusely disperses Cdc42Palm to entire cell (Figure S6B). These findings indicate that palmitoylation results in targeting and transporting Cdc42Palm to the tip of the axon where it modulates axonal length and branching. Compared with WT neurons (n = 64) the normalized intensity of the endogenous Cdc42Palm at the tip of axons is decreased by 19% and 28% in the $Zdhhc8^{+/-}$ (n = 64, $P < 0.02$) and $Zdhhc8^{-/-}$ (n = 67, $P < 0.001$) neurons respectively (Figures 6A and 6B), whereas the area of axon tip displayed no significant change among genotypes (Figure S6C). Reciprocally, Cdc42Palm abundance at axon shafts was increased by 2.1 and 2.9 times in the $Zdhhc8^{+/-}$ (n = 64, $P < 0.0001$) and $Zdhhc8^{-/-}$ (n = 67, $P < 0.0001$) neurons respectively, compared with WT littermates (n = 64) (Figure 6C). Thus, *Zdhhc8* deficiency disrupts the subcellular localization of Cdc42Palm.

To examine the role of endogenous Cdc42Palm in axonal development, an EGFP plasmid-based short hairpin RNA (shRNA) targeting Cdc42Palm was electroporated *ex utero* into E15.5 embryos. We immediately dissected cortices and established primary neuronal cultures to analyze neuronal polarity at DIV3 (Figure S6D and S6E) and axon branching and length at DIV4 (Figure 6D-6G). Whereas most of cells (71%) have a single axon in control scrambled shRNA transfected neurons, Cdc42Palm knockdown displayed a decrease in cells having a single axon (42%, $P < 0.0001$) (Figure S6D and S6E). The axons of Cdc42Palm knockdown neurons were significantly shorter than those of the control cells (60.3 ± 3.9 μm versus 112.1 ± 6.0 μm in WT, $P < 0.0001$; Figure S6F). The length and number of dendrites were also significantly reduced in Cdc42Palm knockdown neurons (Figure S6G and S6H) at DIV3.

In addition, Cdc42Palm knockdown yielded significant reductions of primary axon length (225.3 ± 9.4 μm: n = 32, $P < 0.001$), axon branching (2.0 ± 0.3: n = 32, $P < 0.01$) and total axon length (354.8 ± 26.2 μm: n = 32, $P < 0.01$) compared to scrambled shRNA controls

(primary axon length, 364.4 ± 26.2 μm; axon branching, 3.8 ± 0.5; total axon length, 545.3 ± 47.9 μm: n = 24) at DIV4 (Figures 6D-6G).

To determine the role of Cdc42Palm on axon development *in vivo*, we used *in utero* electroporation of an shRNA targeting Cdc42Palm in newly divided neurons. Following electroporation at E14.5, axonal morphology of neurons was quantified at E17.5. Knockdown of Cdc42Palm resulted in a decrease in axon length (24%, n = 30, $P < 0.0001$) compared with scrambled control shRNA (n = 33) (Figure S6I and S6J). Axon branches in the ipsilateral cortical layers 2–4 in P8.5 brain sections were also quantified, following *in utero* electroporation of the shRNA at E15.5 (Figures 6H and 6I). Cdc42Palm knockdown resulted in a decrease in the number of axonal branches (30%, n = 18, $P < 0.0001$) compared with scrambled control shRNA (n = 18) (Figures 6H and 6I). These results suggest that Cdc42Palm modulates neuronal polarity, axonal elongation and branching.

ZDHHC8 regulates AKT/GSK3 signaling

Three major classes of Cdc42 effectors include N-WASP (neural Wiskott-Aldrich syndrome protein), PAK (p21-activated kinases), which regulate actin polymerization and stabilization as well as PAR (partitioning–defective) proteins, which modulate the PI3K/Akt/Gsk3 signaling pathway and regulate neuronal polarity, axon extension, and branching by transducing upstream signals to reorganization of axonal microtubules (Iden et al., 2008).

The phosphatidylinositol 3-kinase (PI3K) signaling cascade is necessary for axonal growth during polarization (Shi et al., 2003; Schwamborn et al., 2004). PI3K activates Akt by phosphorylation at Thr-308 and Ser-473 via PIP3 phosphoinositide-dependent kinase (Yoshimura et al., 2006). Activated Akt phosphorylates Gsk3β at Ser-9 and inactivate its kinase activity (Yoshimura et al., 2006). Inactivation of Gsk3β is necessary for efficient axon elongation (Zhou et al., 2004). During neuronal polarization, both PI3K and Akt are selectively transported to and enriched at the tip of individual neurites, signaling the progression from nonpolarized stage 2 to polarizing stage 3 (Shi et al., 2003). Localized activation of Cdc42 at the leading edge recruits the Par3-Par6-PKCζ polarity complex, leading to Rac/PI3K activation (Nishimura et al., 2005) or directly binds to the p110β catalytic subunit isoform of PI3K resulting in increased kinase activity and downstream Akt phosphorylation (Fritsch et al., 2013).

We electroporated an shRNA targeting Cdc42Palm *ex utero* into E15.5 embryos and immediately dissected cortices and established primary neuronal cultures (Figure 7A). Quantification confirmed that Cdc42Palm knockdown significantly reduced axon–tip intensity of pAkt (33%, n = 24, $P < 0.001$), compared to control neurons (n = 24) (Figure 7B). As expected, axon–tip intensity of pGsk3β (36%, n = 30, $P < 0.05$) was also reduced by the Cdc42 Palm knockdown (Figures 7C and 7D).

We then asked whether *Zdhhc8* deficiency disrupts the subcellular localization of PI3K, pAkt, and pGsk3β. In stage 3 neurons, *Zdhhc8* deficiency resulted in a slight decrease in pAkt staining within the soma (16%, n = 20, $P < 0.05$) (Figures 7E and 7F). pAkt staining intensity at tip of axon was also decreased by 13% and 24% in the $Zdhhc8^{+/-}$ (n = 20, $P < 0.05$) and $Zdhhc8^{-/-}$ (n = 20, $P < 0.005$) neurons respectively, compared with WT neurons

(n = 20) (Figures 7E and 7F). Similarly, pGsk3β intensity at the tip of axons was also decreased by 14% and 25% in the *Zdhhc8*$^{+/-}$ (n = 20, $P < 0.05$) and *Zdhhc8*$^{-/-}$ (n = 20, $P < 0.003$) neurons respectively, compared with WT neurons (n = 20) (Figures 7G and 7H). Taken together our results suggest that ZDHHC8 is required for optimal Akt/Gsk3β signaling at the tip of the growing axons and that this effect is mediated at least in part via palmitoylation and axonal tip enrichment of Cdc42.

Notably, altered phosphorylation of Akt and Gsk3β, is also evident in western blot assays of PFC lysates of 8 weeks-old *Zdhhc8*-deficient mice. pAkt (Ser473), a marker for Akt activation was reduced 18% and 22% in the PFC of *Zdhhc8*$^{+/-}$ (6 mice, n = 18 , $P < 0.05$) and *Zdhhc8*$^{-/-}$ (6 mice, n =18, $P < 0.005$) respectively, as compared with WT littermates (6 mice, n = 18), (Figures 8A and 8B). pGsk3β (Ser9) was reduced 19% and 29% in the *Zdhhc8*$^{+/-}$ (6 mice, n = 18, $P < 0.005$) and *Zdhhc8*$^{-/-}$ (6 mice, n=18, $P < 0.001$) as compared with WT littermates (6 mice, n =18), respectively (Figures 8A and 8B).

Importantly, *Df(16)A*$^{+/-}$ mice, with only one intact copy of *Zdhhc8*, show a significant reduction in the levels of pAkt (25 % ;12 mice, n = 24, $P < 0.05$) and pGsk3β (19 % ; 12 mice, n = 24, $P < 0.05$), as compared with WT littermates (12 mice) (Figures 8C and 8D).

If alterations of PI3K/Akt/Gsk3β signaling emerge during brain development, we might be able to reverse deficits in axonal branching by decreasing Gsk3β activity in developing *Zdhhc8*$^{-/-}$ mice. To this end, following electroporation with EGFP plasmids at E15.5, pups were treated with DMSO or SB216763 (2 mg/kg i.p.), a Gsk3β inhibitor, every day from P2 to P7. Compared to DMSO treated *Zdhhc8*$^{-/-}$ mice (n = 15, 4 brains), *Zdhhc8*$^{-/-}$ mice treated with SB216763 (n = 15, 4 brains), showed a 50% increase in the number of axon branches in the ipsilateral layers 2/4 (Figures 8E-8G) reaching the number of axon branches in WT mice treated with DMSO (n = 15, 4 brains). Moreover, we observed that contralateral primary axonal branches were increased by 72% in *Zdhhc8*$^{-/-}$ mice treated with SB216763 (n = 16, 4 brains), compared to *Zdhhc8*$^{-/-}$ mice treated with DMSO (n = 12, 4 brains), and restored to the level observed in WT mice treated with DMSO (n = 12, 4 brains) (Figures 8H-8J). These findings establish a causal relationship between altered AKT/GSK3β signaling and *Zdhhc8*-dependent axonal branching *in vivo*.

DISCUSSION

The emerging picture from psychiatric genetics is one of substantial mutational heterogeneity. Modeling in animals a few selected mutations with robust and specific disease associations makes possible gaining insights into fundamental biological mechanisms that underlie disease pathogenesis and pathophysiology. In that context, our study provides a series of novel insights into the mechanisms governing axonal growth and their relation to the psychiatric and cognitive phenotypes associated with a well-established CNV predisposing to schizophrenia. Using a multi-pronged approach, we show that impaired palmitoylation affects axonal growth both *in vitro* and *in vivo* and provide evidence that altered palmitoylation of key axonal proteins emerging as a result of the 22q11.2 deletion results in deficits in axonal arborization and connectivity that affect the formation and function of neural circuits.

Our analysis focuses on ZDHHC8 palmitoyltransferase, encoded by a gene located at the human 22q11.2 deletion locus. Our findings strongly suggests that *Zdhhc8* deficiency accounts for many of the deficits in axonal morphology and synaptic contacts emerging as a result of a hemizygous deletion of the mouse syntenic 22q11.2 locus and reinforce the notion that reduction in the dosage of ZDHHC8 is crucial for establishing altered levels of short and long range connectivity in neurons carrying a deletion of the orthologous 22q11.2 locus.

Identification of bone fide substrates of ZDHHC8, which included a preponderance of proteins involved in axonal growth facilitated elucidation of the mechanistic basis of the observed effects. Although it is very likely that the observed axonal phenotypes are caused by combined underpalmitoylation of more than one of the substrates, we identified a palmitoylated form of Cdc42 (cell division cycle 42), a RhoGTPase previously shown to modulate neuronal polarity and elongation as a key molecular mediator of the effect of altered palmitoylation on axonal growth. Moreover, our genetic and pharmacological rescue analysis provided evidence that the effect of ZDHHC8 on axon growth is mediated in part via Cdc42-dependent modulation of Akt/Gsk3β signaling in the tip of the axon.

Although many psychiatric disorders, such as schizophrenia, emerge during adolescence and early adulthood, behavioral abnormalities including cognitive impairments are often apparent in a portion of patients before diagnostic criteria are met (Brewer et al., 2006). Moreover, genes and cellular pathways implicated in disease risk play important roles both in the developing and mature brain. Both the temporal and spatial expression of ZDHHC8 appears to coincide with peak periods of cortical synaptogenesis, where the enzyme may be critical during late embryogenesis and early postnatal life in establishing formation of short and long range connection of neurons that have migrated into their final destinations. In that respect restoring axonal branching during early postnatal development (by treating mutant pups from P2 to P7 with SB216763) strongly suggests that early intervention that restores the function of this disease pathway may have beneficial effects. However, ZDHHC8 continues to be expressed at high levels in the cortex through adulthood and it remains possible that in addition to its role in the initial formation of cortical circuits, ZDHHC8 function may continue to play an important role in the adult brain in regulating synaptic plasticity of these circuits.

Our results inform both the neural and genetic mechanisms of the disease. First, in schizophrenia and various developmental and psychiatric disorders dysconnectivity between and within brain regions is thought to underlie emergence and severity of symptoms across many psychological domains and brain systems (cognitive, affective, social, motor and perceptual). The exact mechanisms behind the spatiotemporal pattern of dysconnectivity are unknown and likely involve changes in local neural dynamics as well as alterations in anatomical scaffolding (e.g. axonal targeting and synaptogenesis in many brain areas) (Arguello et al., 2012). Our findings advance our understanding of how mutations predisposing to psychiatric and cognitive phenotypes impact circuits and offer one molecular and cellular basis for the structural dysconnectivity in psychiatric and neurodevelopmental disorders implicating the *Zdhhc8* gene and neuronal protein palmitoylation in this process. In that respect, our observation that *Zdhhc8* deficiency can

lead to a specific disruption of vHPC synchrony with the mPFC and impair WM performance was particularly instructive in highlighting the necessity of intact terminal arborization of vHPC projections to mPFC in normal spatial WM. Although appropriately designed rescue studies are needed to establish an unequivocal link between *Zdhhc8* and hippocampal-cortical synchrony, our findings suggest an important role for palmitoylation in shaping efficient long-range connectivity between brain structures.

Second, an emerging view of schizophrenia is that rare alleles contribute significantly to a large proportion of overall genetic risk, whereas secondary modifiers (other rare or common alleles) that regulate the function of key cellular signaling pathways determine the trajectory and severity of the clinical manifestations resulting from a primary disease-causing mutation. In that context, it is worth noting that an increasingly strong link between a dysregulation of Akt and Cdc42 signaling and schizophrenia is emerging in humans and an association between schizophrenia and common Akt1 and Cdc42 genetic variants has been reported in several patient cohorts (Arguello and Gogos, 2008; Gilks et al., 2012; Ide et al., 2010;).

It is also important to consider the implications of our findings for the 22q11.2 locus-associated risk. Existing structural and functional neuroimaging work in 22q11.2 deletion carriers have detected structural abnormalities in white matter volumetric and DTI measures as well as altered resting state functional connectivity (Jalbrzikowski M et al 2014; Baker et al., 2011; Ottet et al., 2013b; Schreiner et al., 2014). Together these studies found an overall global loss of connectivity as well as deficits in long-range connectivity in children with 22q11.2 deletions. Our findings of microscopic structural alterations in axonal branching in conjunction with current and previous finding of altered synaptic transmission and plasticity in cortical synapses of *Df(16)A*$^{+/-}$ mice (Fenelon et al., 2011, 2013) offers a plausible neural substrate that may underlie the mesoscopic scale neuroimaging findings. In addition, there is accumulating data linking neuroimaging measures with the psychosis phenotype in 22q11.2 deletion carriers providing support for the notion that structural and functional dysconnectivity is particularly relevant to the psychosis phenotype in 22q11DS (Kates et al., 2014; Perlstein et al., 2014; Jalbrzikowski M et al 2014; Ottet et al., 2013b). In that respect, our data suggests that the altered axonal connectivity that emerge as a result of deficits in neuronal palmitoylation contribute to the psychiatric deficits associated with the 22q11 deletion. Our findings should be interpreted in the context of decreases in the dosage of neighboring genes that would have a cumulative effect on the properties of neural networks, but the molecular substrates identified here may inform new treatments of the 22q11.2-associated psychiatric symptoms.

Overall, our results demonstrate how bona-fide mutations interact with disease associated signaling pathways that can mediate (and therefore also modify) the effects of a primary mutation on a cellular substrate (axonal connectivity). Translating interaction among primary mutations and signaling pathways at the levels of circuits and neural systems represents a decisive step towards valuable mechanistic insights into the pattern and severity of cognitive and psychiatric symptoms and thus can provide key to understanding genetic and neural mechanisms underlying disease risk.

Experimental Procedures

Zdhhc8* and *Df(16)A*$^{+/-}$ transgenic mice—Zdhhc8* knockout mice were generated and genotyped as previously described (Mukai et al., 2004). The *Df(16)A*$^{+/-}$ mice were generated and genotyped as previously described (Stark et al., 2008). The expected reduction or elimination of *Zdhhc8* transcript levels in the brain was confirmed by quantitative real-time PCR (Mukai et al., 2008). All animal procedures were conducted according to protocols approved by the Institutional Animal Care and Use Committee established by Columbia University under federal and state regulations.

Electroporatlon *in utero*—Pregnant mothers with E14.5 −16.5 embryos were anaesthetized and one inch incision was made and one uterine horn removed. 0.1–0.5 μl DNA (1–2 μg/μl) was injected into one ventricle. 4–5 40–48-volt pulses were applied, each pulse lasting 50 ms, with a 1 second pause between each pulse using an ECM-830 square wave electroporatoror (BTX) as previously described (Saito, 2002).

Drug injection—SB216763 was dissolved in DMSO (20 mg/ml) as the stock solution. Before each injection, the stock solution was freshly diluted to 2 mg/ml with PEG400. Final concentration for each pup is 2 mg/kg. Mice were treated with either control DMSO or SB216763 (2 mg/kg i.p.) every day from P2 to P7 at 9 a.m. Mice were perfused with PBS and 4% Paraformaldehyde at 5 p.m. in P7.

Acyl-biotinyl exchange assay, expression constructs, immunocytochemistry, immunohistochemistry, image acquisition and quantification, cell culture, transfection, and western blot, behavior analysis, electrophysiology and frontal cortex slice preparation are described in detail in **Extended Experimental Procedures**.

Supplementary Material

Refer to Web version on PubMed Central for supplementary material.

Acknowledgments

We thank Naoko Haremaki, Yan Sun, and Megan Sribour for the maintenance of the mouse colony and technical assistance. We are also grateful to Dr. Song-Hai Shi for help with the *in utero* electroporation. We also thank Dr. Manfred W. Kilimann for gift of paralemmin antibody. This work was supported by grants R01MH097879 (to J.A.G). R01MH096274 (to J.G and J.A.G) and MH67068 (M.K. and J.A.G.) JM was partially supported by a NARSAD Young Investigator Award.

References

Arguello PA, Gogos JA. A signaling pathway AKTing up in schizophrenia. J. Clin. Invest. 2008; 118:2018–2021. [PubMed: 18497888]

Arguello PA, Gogos JA. Genetic and cognitive windows into circuit mechanisms of psychiatric disease. Trends Neurosci. 2012; 35:3–13. [PubMed: 22177981]

Baker K, Chaddock CA, Baldeweg T, Skuse D. Neuroanatomy in adolescents and young adults with 22q11 deletion syndrome: comparison to an IQ-matched group. Neuroimage. 2011; 55:491–499. [PubMed: 21184831]

Bearden CE, Woodin MF, Wang PP, Moss E, McDonald-McGinn D, Zackai E, Emannuel B, Cannon TD. The neurocognitive phenotype of the 22q11.2 deletion syndrome: selective deficit in visual-spatial memory. J. Clin. Exp. Neuropsychol. 2001; 23:447–464. [PubMed: 11780945]

Brewer WJ, Wood SJ, Phillips LJ, Francey SM, Pantelis C, Yung AR, Cornblatt B, McGorry PD. Generalized and specific cognitive performance in clinical high-risk cohorts: a review highlighting potential vulnerability markers for psychosis. Schizophr. Bull. 2006; 32:538–555. [PubMed: 16782759]

Chen WY, Shi YY, Zheng YL, Zhao XZ, Zhang GJ, Chen SQ, Yang PD, He L. Case-control study and transmission disequilibrium test provide consistent evidence for association between schizophrenia and genetic variation in the 22q11 gene ZDHHC8. Hum. Mol. Genet. 2004; 13:2991–2995. [PubMed: 15489219]

Courchet J, Lewis TL Jr, Lee S, Courchet V, Liou DY, Aizawa S, Polleux F. Terminal axon branching is regulated by the LKB1-NUAK1 kinase pathway via presynaptic mitochondrial capture. Cell. 2013; 153:1510–1525. [PubMed: 23791179]

el-Husseini AE, Bredt DS. Protein palmitoylation: a regulator of neuronal development and function. Nat. Rev. Neurosci. 2002; 3:791–802. [PubMed: 12360323]

Fénelon K, Mukai J, Xu B, Hsu PK, LJ, Karayiorgou M, Fischbach GD, Macdermott AB, Gogos JA. Deficiency of Dgcr8, a gene disrupted by the 22q11.2 microdeletion, results in altered short-term plasticity in the prefrontal cortex. Proc. Natl. Acad. Sci. U. S. A. 2011; 108:4447–4452. [PubMed: 21368174]

Fénelon K, Xu B, Lai CS, Mukai J, Markx S, Stark KL, Hsu PK, Gan WB, Fischbach GD, MacDermott AB, Karayiorgou M, Gogos JA. The pattern of cortical dysfunction in a mouse model of a schizophrenia-related microdeletion. J. Neurosci. 2013; 33:14825–14839. [PubMed: 24027283]

Fritsch R, de Krijger I, Fritsch K, George R, Reason B, Kumar MS, Diefenbacher M, Stamp G, Downward J. RAS and RHO Families of GTPases Directly Regulate Distinct Phosphoinositide 3-Kinase Isoforms. Cell. 2013; 153:1050–1063. [PubMed: 23706742]

Fukata M, Fukata Y. Protein palmitoylation in neuronal development and synaptic plasticity. Nat. Rev. Neurosci. 2010; 3:161–175. [PubMed: 20168314]

Garvalov BK, Flynn KC, Neukirchen D, Meyn L, Teusch N, Wu X, Brakebusch C, Bamburg JR, Bradke F. Cdc42 regulates cofilin during the establishment of neuronalpolarity. J. Neurosci. 2007; 27:13117–13129. [PubMed: 18045906]

Gilks WP, Hill M, Gill M, Donohoe G, Corvin AP, Morris DW. Functional investigation of a schizophrenia GWAS signal at theCDC42 gene. World J. Biol. Psychiatry. 2012; 13:550–554. [PubMed: 22385474]

Ho GP, Selvakumar B, Mukai J, Hester LD, Wang Y, Gogos JA, Snyder SH. S-nitrosylation and S-palmitoylation reciprocally regulate synaptic targeting of PSD-95. Neuron. 2011; 71:131–141. [PubMed: 21745643]

Ide M, Lewis DA. Altered cortical CDC42 signaling pathways in schizophrenia: implications for dendritic spine deficits. Biol. Psychiatry. 2010; 68:25–32. [PubMed: 20385374]

Iden S, Collard JC. Crosstalk between small GTPases and polarity proteins in cell polarization. Mol. Cell Biol. 2008; 9:846–859.

Jalbrzikowski M, Villalon-Reina JE, Karlsgodt KH, Senturk D, Chow C, Thompson PM, Bearden CE. Altered white matter microstructure is associated with social cognition and psychotic symptoms in 22q11.2 microdeletion syndrome. Front. Behav. Neurosci.. 2014; 8:393. [PubMed: 25426042]

Jeanneteau F, Deinhardt K, Miyoshi G, Bennett AM, Chao MV. The MAP kinase phosphatase MKP-1 regulates BDNF-induced axon branching. Nat. Neurosci. 2010; 13:1373–1379. [PubMed: 20935641]

Kanaan R, Barker G, Brammer M, Giampietro V, Shergill S, et al. White matter microstructure in schizophrenia: effects of disorder, duration and medication. Br. J. Psychiatry. 2009; 194:236–242. [PubMed: 19252154]

Kanaan RA, Borgwardt S, McGuire PK, Craig MC, Murphy DG, Picchioni M, Shergill SS, Jones DK, Catani M. Microstructural organization of cerebellar tracts in schizophrenia. Biol. Psychiatry. 2009; 66:1067–1069. [PubMed: 19733836]

Kang R, Wan J, Arstikaitis P, Takahashi H, Huang K, Bailey AO, Thompson JX, Roth AF, Drisdel RC, Mastro R, et al. Neural palmitoyl-proteomics reveals dynamic synaptic palmitoylation. Nature. 2008; 456:904–909. [PubMed: 19092927]

Kates WR, Olszewski AK, Gnirke MH, Kikinis Z, Nelson J, Antshel K, et al. White matter microstructural abnormalities of the cingulum bundle in youths with 22q11.2 deletion syndrome: associations with medication, neuropsychological function, and prodromal symptoms of psychosis. Schizophr. Res. 2015; 161:76–84. [PubMed: 25066496]

McDonald-McGinn DM, Tonnesen MK, Laufer-Cahana A, Finucane B, Driscoll DA, Emanuel BS, Zackai EH. Phenotype of the 22q11.2 deletion in individuals identified through an affected relative: cast a wide FISHing net! Genet. Med. 2001; 3:23–29.

Mukai J, Liu H, Burt RA, Swor DE, Lai WS, Karayiorgou M, Gogos JA. Evidence that the gene encoding ZDHHC8 contributes to the risk of schizophrenia. Nat. Genet. 2004; 36:725–731. [PubMed: 15184899]

Mukai J, Dhilla A, Drew LJ, Stark KL, Cao L, MacDermott AB, Karayiorgou M, Gogos JA. Palmitoylation-dependent neurodevelopmental deficits in a mouse model of 22q11 microdeletion. Nat. Neurosci. 2008; 11:1302–1310. [PubMed: 18836441]

Nishimura A, Linder ME. Identification of a novel prenyl and palmitoyl modification at the CaaX motif of Cdc42 that regulates RhoGDI binding. Mol. Cell. Biol. 2013; 33:1417–1429. [PubMed: 23358418]

Nishimura T, Yamaguchi T, Kato K, Yoshizawa M, Nabeshima Y, Ohno S, Hoshino M, Kaibuchi K. PAR-6-PAR-3 mediates Cdc42-induced Rac activation through the Rac GEFs STEF/Tiam1. Nat. Cell. Biol. 2005; 7:270–277. [PubMed: 15723051]

Ottet M-C, Schaer M, Debbané M, Cammoun L, Thiran J-P, Eliez S. Graph theory reveals dysconnected hubs in 22q11DS and altered nodal efficiency in patients with hallucinations. Front. Hum. Neurosci. 2013; 7:402. [PubMed: 24046733]

Perlstein MD, Chohan MR, Coman IL, Antshel KM, Fremont WP, Gnirke MH, et al. White matter abnormalities in 22q11.2 deletion syndrome: preliminary associations with the Nogo-66 receptor gene and symptoms of psychosis. Schizophr. Res. 2014; 152:117–123. [PubMed: 24321711]

Pulver AE, Nestadt G, Goldberg R, Shprintzen RJ, Lamacz M, Wolyniec PS, Morrow B, Karayiorgou M, Antonarakis SE, Housman D, et al. Psychotic illness in patients diagnosed with velo-cardio-facial syndrome and their relatives. J. Nerv. Ment. Dis. 1994; 182:476–478. [PubMed: 8040660]

Scheiner MJ, Karlsgodt KH, Uddin LQ, Chow C, Congdon E, Jalbrzikowski M, Bearden CE. Default mode network connectivity and reciprocal social behavior in 22q11.2 deletion syndrome. Soc Cogn Affect Neurosci. 2014; 9:1261–1267. [PubMed: 23912681]

Shi SH, Jan LY, Jan YN. Hippocampal neuronal polarity specified by spatially localized mPar3/mPar6 and PI 3-kinase activity. Cell. 2003; 112:63–75. [PubMed: 12526794]

Sigurdsson T, Stark KL, Karayiorgou M, Gogos JA, Gordon JA. Impaired hippocampal-prefrontal synchrony in a mouse model of schizophrenia. Nature. 2010; 464:763–766. [PubMed: 20360742]

Stark KL, Xu B, Bagchi A, Lai WS, Liu H, Hsu R, Wan X, Pavlidis P, Mills AA, Karayiorgou M, Gogos JA. Altered brain microRNA biogenesis contributes to phenotypic deficits in a 22q11-deletion mouse model. Nat. Genet. 40:751–760. [PubMed: 18469815]

Tahirovic S, Hellal F, Neukirchen D, Hindges R, Garvalov BK, Flynn KC, Stradal TE, Chrostek-Grashoff A, Brakebusch C, Bradke F. Rac1 regulates neuronal polarization through the WAVE complex. J. Neurosci. 2010; 30:6930–6943. [PubMed: 20484635]

Thomas GM, Hayashi T, Chiu SL, Chen CM, Huganir RL. Palmitoylation by DHHC5/8 targets GRIP1 to dendritic endosomes to regulate AMPA-R trafficking. Neuron. 2012; 73:482–496. [PubMed: 22325201]

Yoshii A, Murata Y, Kim J, Zhang C, Shokat KM, Constantine-Paton M. TrkB and protein kinase Mζ regulate synaptic localization of PSD-95 in developing cortex. J Neurosci. 2011; 31:11894–11904. [PubMed: 21849550]

Yoshimura T, Arimura N, Kaibuchi K. Signaling networks in neuronal polarization. J Neurosci. 2006; 26:10626–10630. [PubMed: 17050700]

Wan J, Roth AF, Bailey AO, Davis NG. Palmitoylated proteins: purification and identification. Nat. Protoc. 2007; 2:1573–1584. [PubMed: 17585299]

Wirth A, Chen-Wacker C, Wu YW, Gorinski N, Filippov MA, Pandey G, Ponimaskin E. Dual lipidation of the brain-specific Cdc42 isoform regulates its functional properties. Biochem. J. 2013; 456:311–322. [PubMed: 24059268]

Woodin M, Wang PP, Aleman D, MacDonald-Mcginn D, Zackal E, Mose E. Neuropsychological profile of children and adolescents with the 22q11.2 microdeletion. Genet. Med. 2001; 3:34–39. [PubMed: 11339375]

Xu B, Roos JL, Levy S, van Rensburg EJ, Gogos JA, Karayiorgou M. Strong association of de novo copy number mutations with sporadic schizophrenia. Nat. Genet. 2008; 40:880–885. [PubMed: 18511947]

Zhou FQ, Zhou J, Dedhar S, Wu YH, Snider WD. NGF-induced axon growth is mediated by localized inactivation of GSK-3beta and functions of the microtubule plus end binding protein APC. Neuron. 2004; 42:897–912. [PubMed: 15207235]

1. The *ZDHHC8* gene within the 22q11.2 deletion controls axonal growth and branching.
2. Palmitoylation of CDC42 by ZDHHC8 promotes axon branching via AKT/GSK3β signaling
3. Zdhhc8-deficiency alters short and long-range connectivity and working memory.
4. Pharmacological decrease of Gsk3β activity during development reverses axonal deficits.

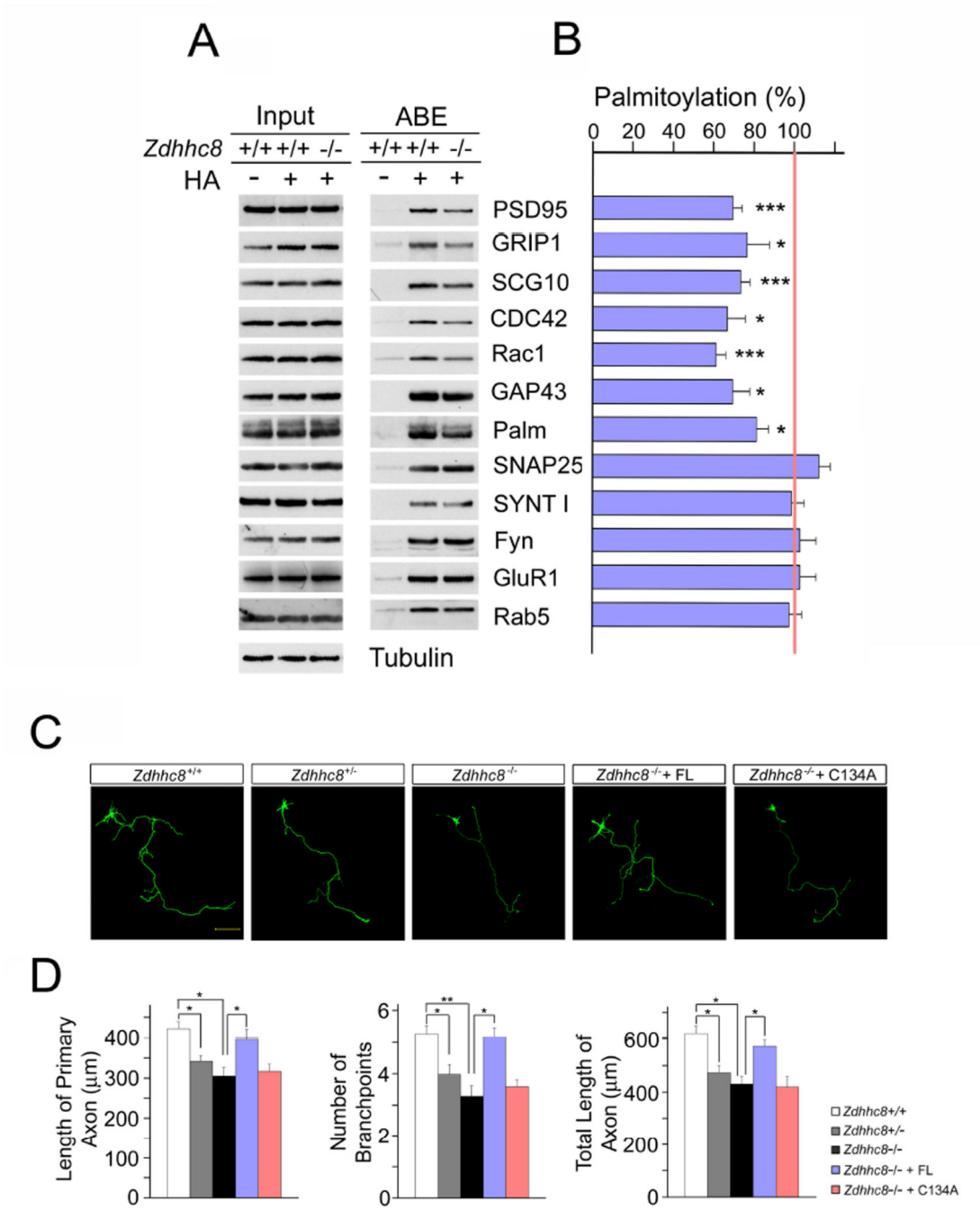

Figure 1. Acyl-biotinyl exchange (ABE) analysis of neuronal protein palmitoylation and axonal alterations in *Zdhhc8*-deficient cortical neurons

(**A**) Palmitoylation levels of selected palmitoyl protein candidate substrates. Proteins, ABE-purified from cultured cortical neurons from WT and *Zdhhc8*$^{-/-}$ mice, both in the presence (+) and absence (-) of hydroxylamine (HA), were analyzed by western blotting using the indicated specific antibodies. Palmitoylated proteins are expected to show HA-dependent detection. As a control, a portion of the starting protein sample (prior to ABE purification) was also screened. Palm, paralemmin; SYNT I, synaptotagmin I.

(B) Quantification of the palmitoylation changes induced by *Zdhhc8*$^{-/-}$ deficiency. Protein levels measured from the purified palmitoyl-protein samples were normalized to levels measured from the corresponding input of substrates.

(**C**) Representative images of *Zdhhc8*-dependent axonal deficits in cortical neurons expressing EGFP at DIV4. *Zdhhc8*$^{-/-}$ cortical neurons were transfected with plasmids expressing EGFP and ZDHHC8-FL or ZDHHC8-C134A at DIV2 and fixed at DIV4. Scale bar, 50 μm.

(**D**) Quantification of axon length and branch points number *in Zdhhc8*-deficient cortical neurons. Transfection of ZDHHC8-FL, but not ZDHHC8-C134A, restored axon length and branchpoints number. Data are shown as means ± s.e.m. *, $P < 0.05$; **, $P < 0.001$; ***, $P < 0.0001$; Student's t-test.

See also Figure S1.

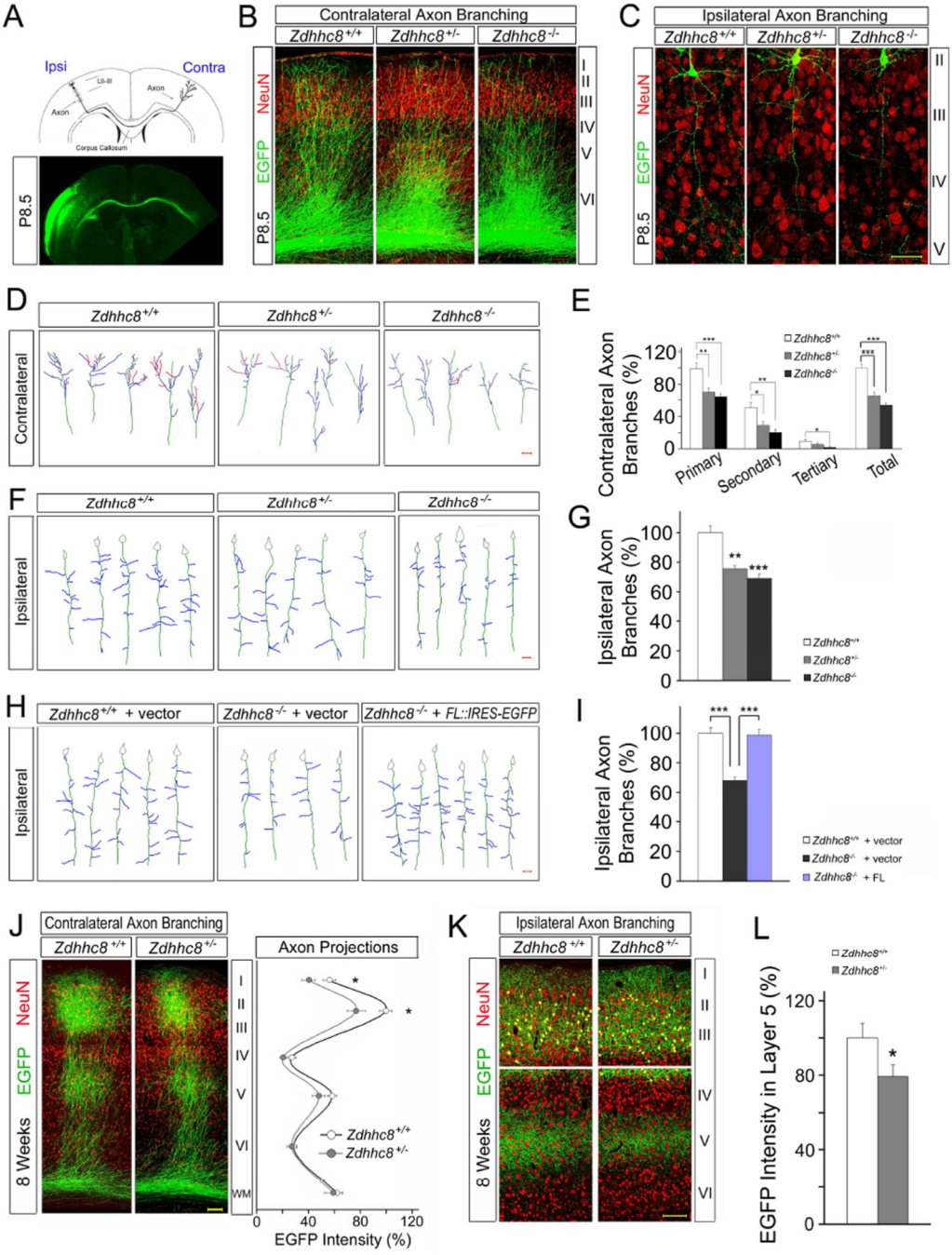

Figure 2. Downreguration of *Zdhhc8* disrupts axonal growth *in vivo*

(**A**) Illustration of the callosal axon pathway of neurons residing at layers 2/3, electroporated with EGFP at E15.5 and assayed at P8.5 (upper panel). Lower panel shows EGFP-labeled neurons.

(**B, C**) Representative images of contralateral axon terminal branching (B) and ipsilateral axon branching (C) of EGFP–labeled neurons from coronal sections of P8.5 brains of mice *in utero* electroporated at E15.5.

(**D**) Tracings of representative neurons in *in utero* electroporated brains expressing EGFP at P8.5, from similar sections as in (B). Depicted are 2D projections of the axon terminal in the contralateral cortical layers 1–4. Primary (blue), secondary (red), and tertiary (pink) branches from axons (green) are highlighted. Scale bar, 20 μm.
(**E**) Quantitative assessment of contralateral axon branching in layers 1–4 reveals a reduction of branch number in *Zdhhc8*-deficient mice.
(**F**) Tracings of representative neurons in *in utero* electroporated brains expressing EGFP at P8.5, from similar sections as in (**C**). Depicted are 2D projections of the axon branching in the ipsilateral cortical layers 2–4. Primary (blue) branches from axon (green) and soma (grey) are highlighted. Scale bar, 20 μm.
(**G**) Quantification of axon branch numbers in the ipsilateral layers 2–4 reveals a reduction of branch number in *Zdhhc8*-deficient mice.
(**H**) Tracings of representative neurons, depicting 2D projection of the ipsilateral axonal arbor in layers 2–4 from brains *in utero* electroporated with either *IRES-EGFP* vector (*Zdhhc8*$^{-/-}$ and WT mice) or *ZDHHC8FL::IRES-EGFP* (*Zdhhc8*$^{-/-}$ mice). Scale bar, 20 μm.
(**I**) Quantification of axonal branch numbers in the ipsilateral layers 2–4, electroporated with either *IRES-EGFP* vector (*Zdhhc8*$^{-/-}$ and WT mice) or *ZDHHC8FL::IRES-GFP* (*Zdhhc8*$^{-/-}$ mice). ZDHHC8-FL restored axonal branch numbers in the ipsilateral layers 2–4 of *Zdhhc8*$^{-/-}$ mice. **(J)** Representative images of contralateral axon terminal branching of EGFP–labeled neurons from coronal sections of P56 brains of mice *in utero* electroporated at E15.5 (*left panel*). Right panel depicts a quantitative assessment of contralateral axon branching in layers 1–6 and the white matter at P56 indicating a reduction of branch number in layers 1 and 2/3 in *Zdhhc8*$^{+/-}$mice (n = 25, 6 brains), compared to *Zdhhc8*$^{+/+}$ mice (n = 20, 5 brains).
(**K**) Representative images of ipsilateral axon branching of EGFP–labeled neurons from coronal sections of P56 brains of mice *in utero* electroporated at E15.5.
(**L**) Quantitative assessment of ipsilateral axon branching in layer 5 at P56 reveals a reduction of branch number in *Zdhhc8*$^{+/-}$ mice (n = 24, 6 brains), compared to *Zdhhc8*$^{+/+}$ mice (n = 24, 5 brains).
Data are shown as means ± s.e.m. * $P < 0.05$; ** $P < 0.001$; *** $P < 0.0001$; Student's t-test. See also Figure S2.

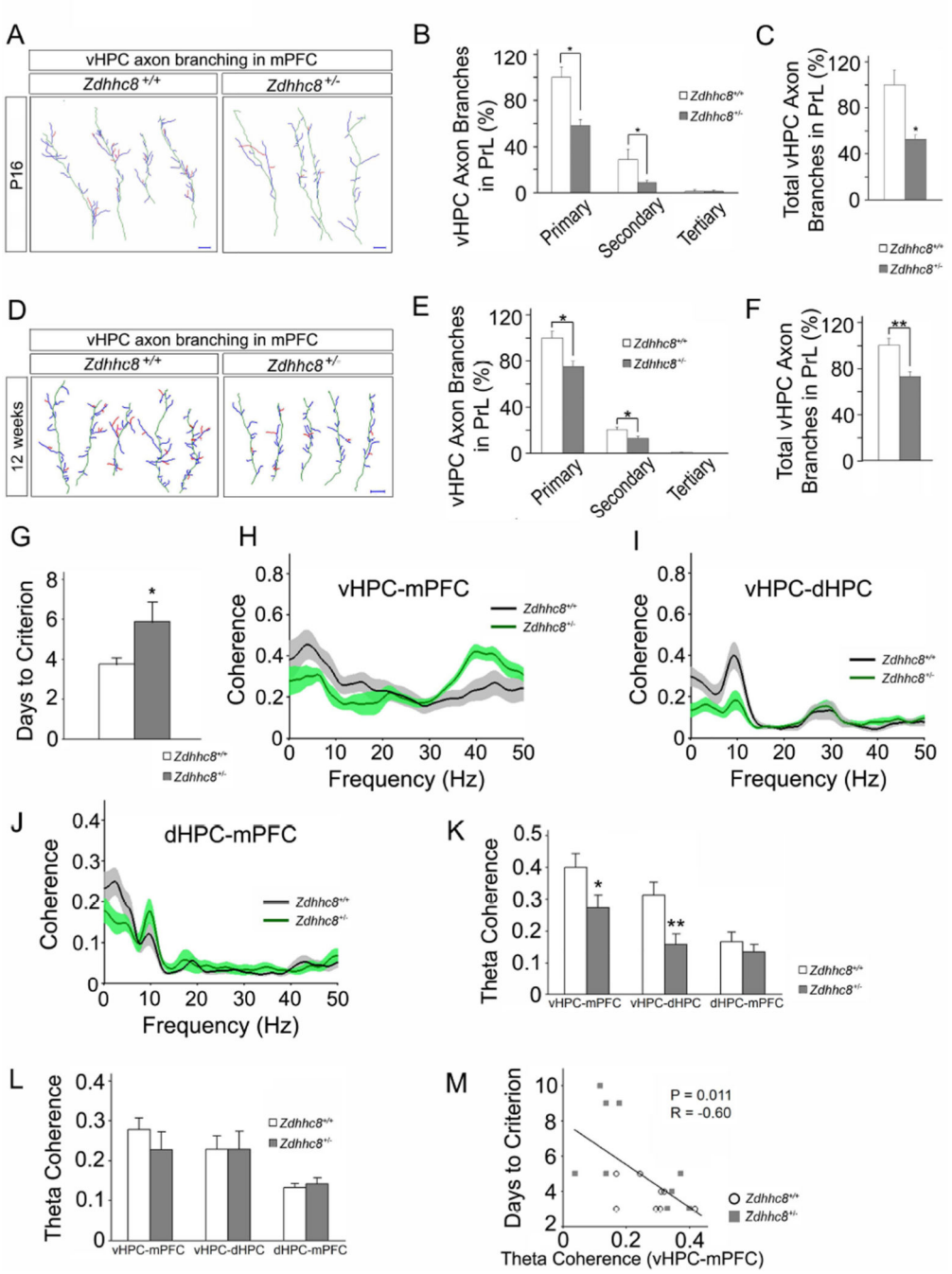

Figure 3. *Zdhhc8* haploinsufficiency impairs spatial working memory and prefrontal-hippocampal synchrony

(**A**) Tracings of representative vHPC neurons from *Zdhhc8* mouse brains (Figure S3J), *in utero* electroporated an EGFP construct to vHPC at E16.5, depicting 2D projection of the axon terminal in the prelimbic layer 5 at P16. Primary (blue), secondary (red), and tertiary (pink) branches from axons (green) are highlighted. Scale bar, 50 μm.

(**B**) Quantitative assessment of vHPC axon branching in prelimbic layer 5 results in a reduction of branch number in *Zdhhc8*$^{+/-}$ mice ($P < 0.05$, n = 18, 6 animals), compared to

Zdhhc8$^{+/+}$ mice (n = 18, 5 animals). Graph showing the proportion of branches of different order in axon arbors.

(**C**) Total branch number in prelimbic layer 5 results in a reduction of branch number in *Zdhhc8*$^{+/-}$ mice ($P < 0.05$, n = 18, 6 animals), compared to *Zdhhc8*$^{+/+}$ mice (n = 18, 5 animals).

(D) Tracings of representative vHPC neurons from *Zdhhc8* mouse brains (Figure S3L), injected rAAV1/hSynapsin/EGFP to vHPC at P56, depicting 2D projection of the axon terminal in the prelimbic layer 5 at P84 (12 weeks). Primary (blue), secondary (red), and tertiary (pink) branches from axons (green) are highlighted. Scale bar, 20 μm.

(E) Quantitative assessment of vHPC axon branching in prelimbic layer V results in a reduction of branch number in *Zdhhc8*$^{+/-}$ mice ($P < 0.05$, n = 20, 4 animals), compared to *Zdhhc8*$^{+/+}$ mice (n = 20, 4 animals). Graph showing the proportion of different order branches in axon arbors.

(**F**) Total branch number in prelimbic layer 5 results in a reduction of branch number in *Zdhhc8*$^{+/-}$ mice ($P < 0.001$, n = 20, 4 animals), compared to *Zdhhc8*$^{+/+}$ mice (n = 20, 4 animals).

(**G**) Days taken to reach criterion performance (three consecutive days of >70% choice accuracy) on the delayed non-match to sample T-maze task.

(**H-K**) Averaged coherence spectra between each pair of brain regions, vHPC-mPFC (**H**), vHPC-dHPC (**I**), and dHPC-mPFC (**J**), during the choice phase after acquisition of the task. Shaded areas are ± s.e.m (**H-J**). Theta-frequency coherence by genotype for each region pair (**K**). (**L**) Baseline theta coherence between each pair of regions during habituation before training. (**M**) Relationship between days to criterion and baseline theta coherence between vHPC and mPFC. n = 8 and 9 animals for WT and *Zdhhc8*$^{+/-}$ mice. *$P < 0.05$, **$P < 0.01$; Student's t-test. Data are means ± s.e.m.

See also Figure S3.

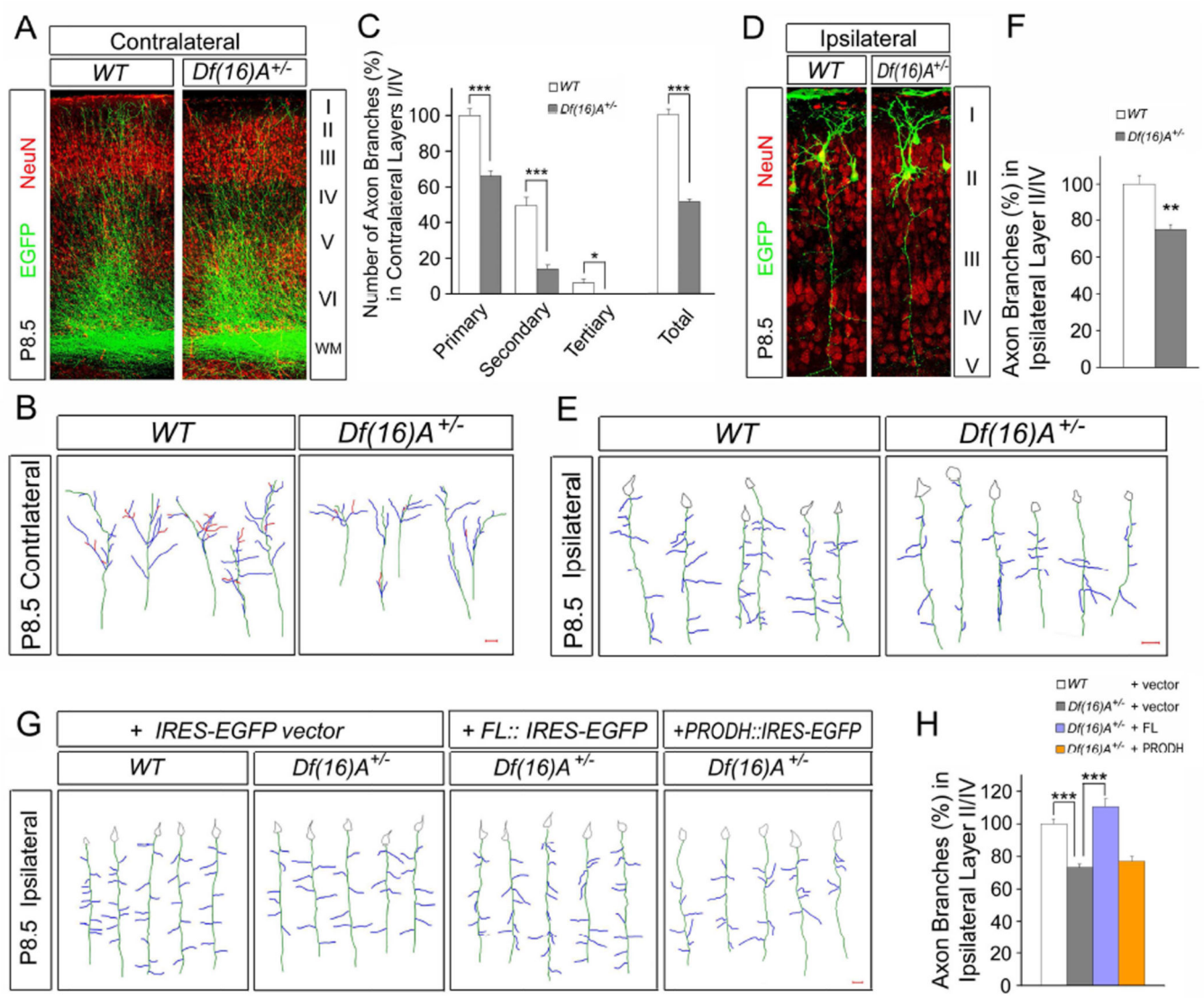

Figure 4. Axonal growth is disrupted in *Df16(A)*$^{+/-}$ mice

(**A**) Confocal images of contralateral axon terminal branching of EGFP–labeled neurons from coronal sections of P8.5 brains of mice *in utero* electroporated at E15.5.

(**B**) Tracings of representative neurons from similar sections as in (A), depicting 2D projection of the axon terminal in the contralateral cortical layers 1–4 from *in utero* electroporated brains expressing EGFP at P8.5. Primary (*blue*), secondary (*red*), and tertiary (*pink*) branches from axons (*green*) are highlighted.

(**C**) Quantification of contralateral axon terminal branch numbers in the layers 1–4 reveals a reduction of branch number in *Df16(A)*$^{+/-}$ (n = 33, 5 brains), compared control mice brains (n = 22, 6 brains).

(**D**) Confocal images of ipsilateral axon branching of EGFP–labeled neurons from coronal sections of P8.5 brains of mice *in utero* electroporated at E15.5.

(**E**) Tracings of representative neurons in *in utero* electroporated brains expressing EGFP at P8.5, from similar sections as in (D). Depicted are 2D projections of the axon branching in the ipsilateral cortical layers 2–4.

(**F**) Quantification of axon branch numbers in the ipsilateral layers 2–4 reveals a reduction of branch number in *Df16(A)*$^{+/-}$ (n = 18, 5 brains), compared control mice brains (n = 18, 6 brains).

(**G**) Tracings of representative neurons, depicting 2D projection of the ipsilateral axonal arbor in layers 2–4 from brains *in utero* electroporated with either *IRES-EGFP* vector (*Df16(A)*$^{+/-}$, and WT mice) or *ZDHHC8FL::IRES-EGFP* (*Df16(A)*$^{+/-}$ mice) or *PRODH::IRES-EGFP* (*Df16(A)*$^{+/-}$mice).

(**H**) Quantification of axonal branch numbers in the ipsilateral layers 2–4 of brains electroporated with either *IRES-EGFP* vector [*Df16(A)*$^{+/-}$ (n = 18, 4 brains) and WT mice (n = 18, 5 brains)] or *ZDHHC8FL::IRES-GFP* [*Df16(A)*$^{+/-}$ mice (n = 18, 4 brains)], or *PRODH::IRES-EGFP* [*Df16(A)*$^{+/-}$ mice (n = 30, 4 brains)]. ZDHHC8-FL restored axonal branch numbers in the ipsilateral layers 2–4 in *Df16(A* $^{+/-}$ mice.

Data are shown as means ± s.e.m. * $P < 0.05$; ** $P < 0.001$; *** $P < 0.0001$; Student's t-test. See also Figure S4.

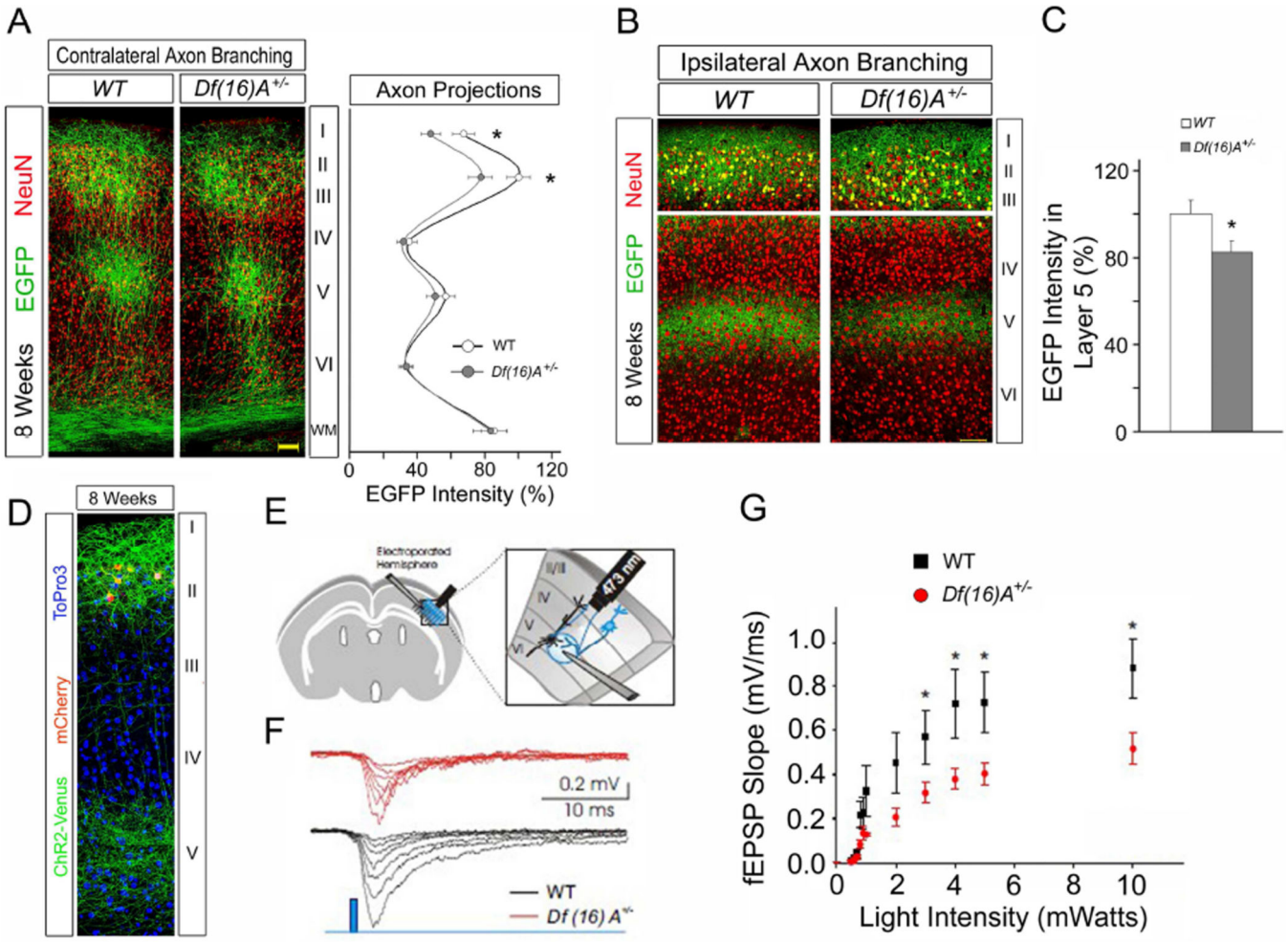

Figure 5. Disrupted axonal branching and synaptic transmission in the adult brain of *Df16(A)*$^{+/-}$ mice

(A) Representative images of contralateral axon terminal branching of EGFP–labeled neurons from coronal sections of P56 (8 weeks) brains of mice *in utero* electroporated at E15.5 (*left panel*). Right panel depicts that a quantitative assessment of contralateral axon branching in layers 1–6 and white matter at P56 indicating a reduction of branch number in layers 1 and 2/3 in *Df16(A)*$^{+/-}$ mice (n = 18, 4 brains), compared to WT mice (n = 20, 5 brains).

(**B**) Representative images of ipsilateral axon branching of EGFP–labeled neurons from coronal sections of P56 (8 weeks) brains of mice *in utero* electroporated at E15.5.

(**C**) Quantitative assessment of ipsilateral axon branching in layer 5 at P56 reveals a reduction of branch number in *Df16(A)*$^{+/-}$ mice (n = 18, 4 brains), compared to WT mice (n = 18, 5 brains).

(**D**) Confocal image of ChR2-Venus expressing neurons residing in the layer 2 from *in utero* electroporated brains at 8 weeks.

(E) Schematic drawing illustrating a coronal section of the mouse frontal cortex, *in utero* electroporated ChR2-Venus with mCherry to layer 2 neurons. Extracellular electrophysiological recordings were performed at the ipsilateral layers 2–5 synapses.

(F) Pulses of blue light (488 nm) were used to evoke fEPSPs that were quantified by measuring the initial slope. Examples traces of light-evoked fEPSPs are shown for both genotypes at photostimulation of increasing intensity.

(G) Summary of the optically-evoked fEPSPs at layers 2–5 synapses in the frontal cortex of WT (N = 7, n = 16; *black squares*) and *Df(16)A*$^{+/-}$ mice (N = 4, n = 11, *red circles*) at different stimulation intensities. The fEPSP of *Df(16)A*$^{+/-}$ mice are smaller at higher stimulations intensities (3–10 mWatts, $P < 0.05$).

See also Figure S5.

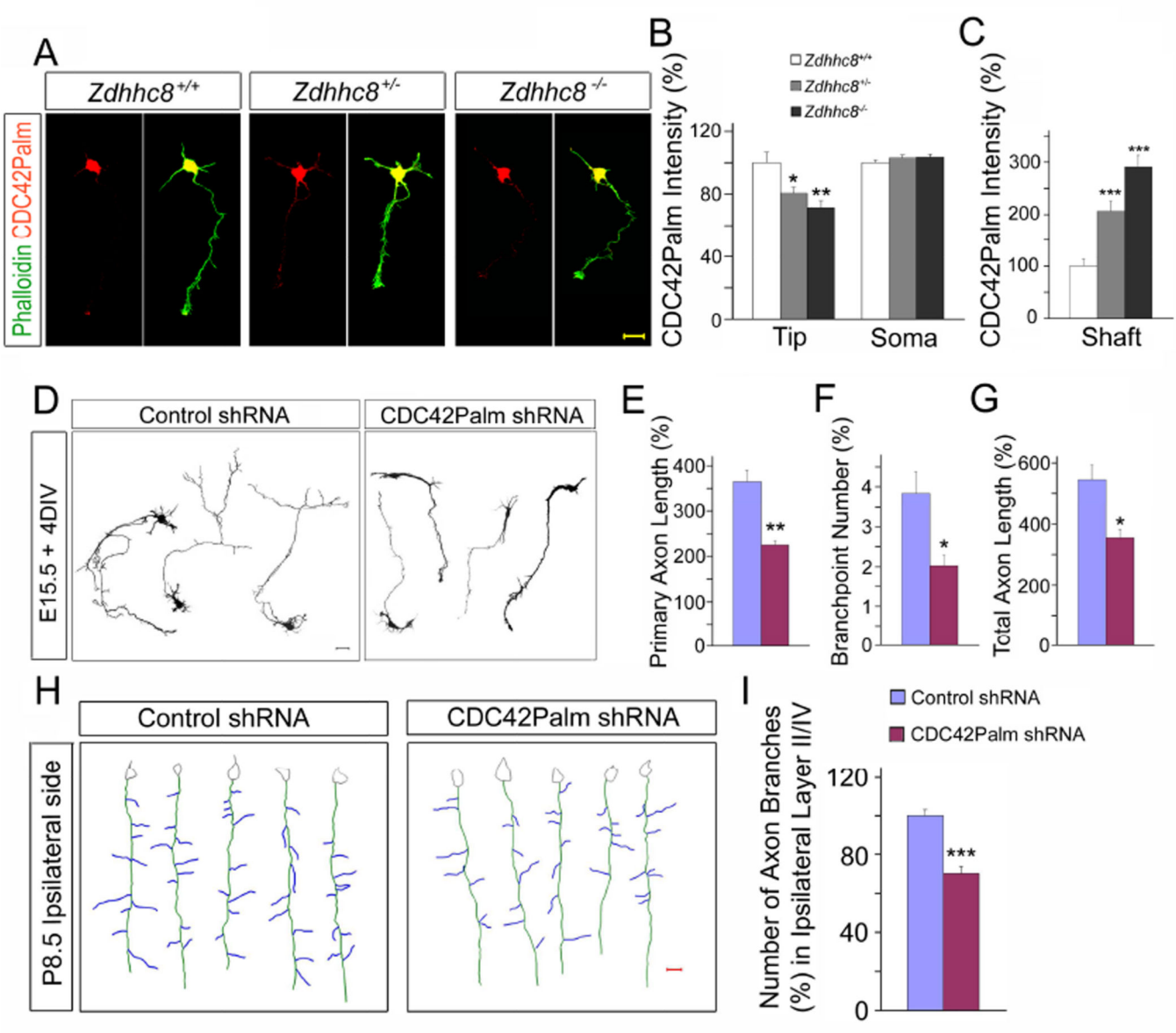

Figure 6. *Zdhhc8* deficiency disrupts tip localization of CDC42Palm

(**A**) Representative images of DIV3 cortical neurons from *Zdhhc8*-deficient mice, immunostained for CDC42Palm (*red*) and phalloidin (*green*).

(**B, C**) Quantification of endogenous CDC42Palm fluorescent intensity in DIV3 *Zdhhc8*-deficient neurons reveals a reduction at the tip of axon (B), and a reciprocal increase at the axon shaft (C).

(**D**) Tracings of representative neurons imaged at DIV4 following *ex utero* electroporation of an shRNA targeting CDC42Palm or a control scrambled shRNA. Scale bar = 20 μm.

(**E-G**) Quantification of axon morphology reveals that knockdown of CDC42Palm results in a shortened axon and decreased branches.

(**H**) Tracings of representative neurons from coronal sections of C57 brains at P8.5, *in utero* electroporated with an shRNA targeting CDC42Palm or a control scrambled shRNA at

E15.5, depicting 2D projection of the axon branching in the ipsilateral cortical layers 2–4. Scale bar, 20 μm.

(**I**) Quantification of axon branch numbers in the ipsilateral layers 2–4 reveals that knockdown of CDC42Palm results in a reduction of branch numbers.

Data are shown as means ± s.e.m. *, $P < 0.05$; **, $P < 0.001$; ***, $P < 0.0001$; Student's t-test.

See also Figure S6.

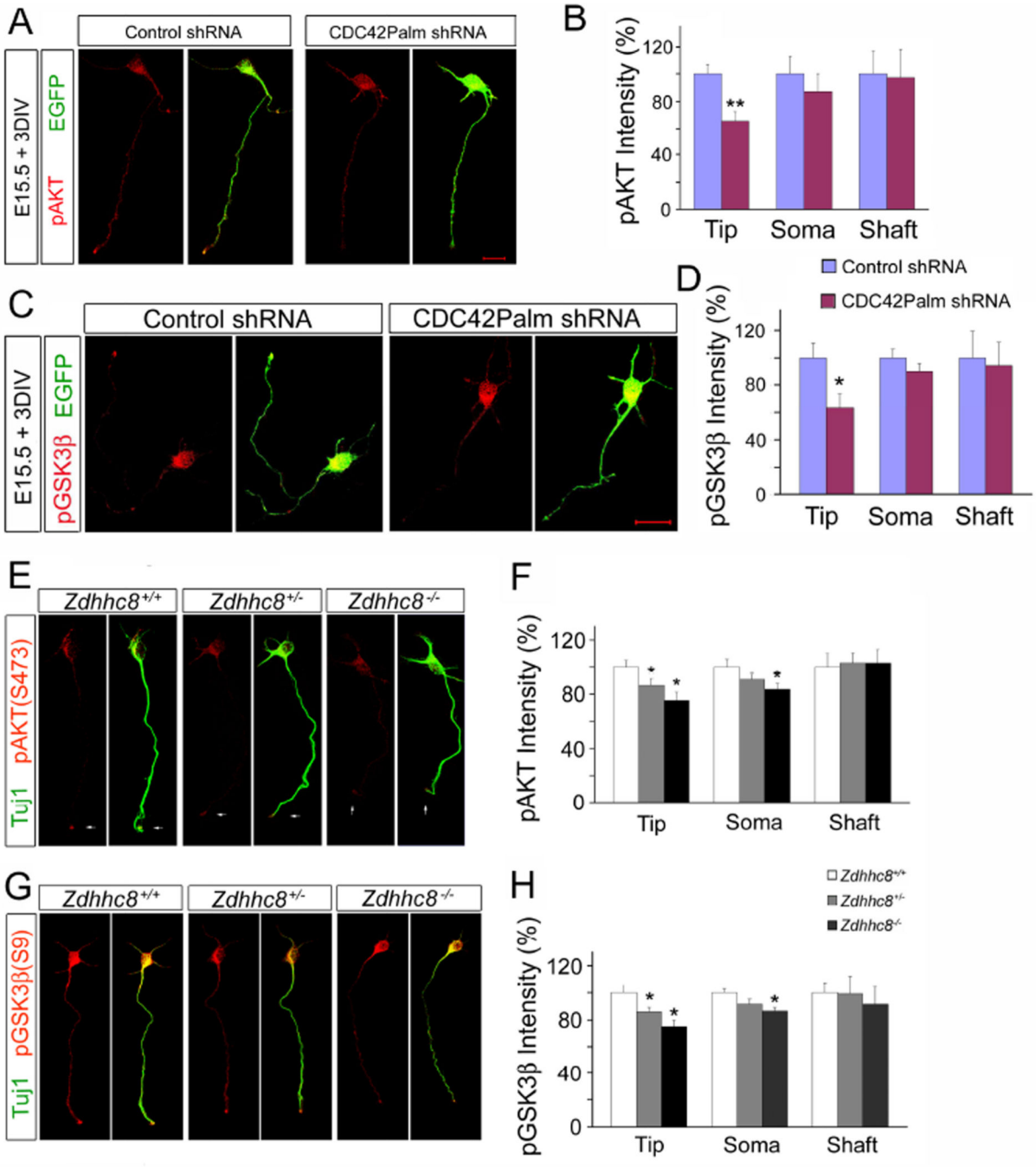

Figure 7. *Zdhhc8* deficiency disrupts AKT/GSK3β signaling cascade

(**A**) Representative cortical neurons stained for pAKT (S473) (*red*) and EGFP (*green*) at DIV3 following *ex utero* electroporation of shRNA targeting CDC42Palm or scrambled shRNA.

(**B**) Quantification of fluorescence intensity reveals that knockdown of CDC42Palm reduces pAKT (S473) intensity at the tip of the axon.

(**C**) Representative cortical neurons stained for pGSK3β (S9) (*red*) and EGFP (*green*) at DIV3 following *ex utero* electroporation of shRNA targeting CDC42Palm or scrambled shRNA.

(**D**) Quantification of fluorescence intensity reveals that knockdown of CDC42Palm reduces pGSK3β (S9) intensity at the tip of the axon.

(**E**) Representative images of DIV3 cortical neurons immunostained with pAKT(S473) (*red*) and neuronal marker Tuj1(*green*) from *Zdhhc8*-deficient and control mice.

(**F**) Quantification of fluorescence intensity reveals that *Zdhhc8* deficiency reduces pAKT(S473) intensity at the tip of axon.

(**G**) Representative images of DIV3 cortical neurons immunostained with pGSK3β(S9) (*red*) and neuronal marker Tuj1(*green*) from *Zdhhc8*-deficient and control mice.

(**H**) Quantification of axon tip fluorescence intensity reveals that *Zdhhc8* deficiency reduces pGSK3b(S9) intensity at the tip of axon.

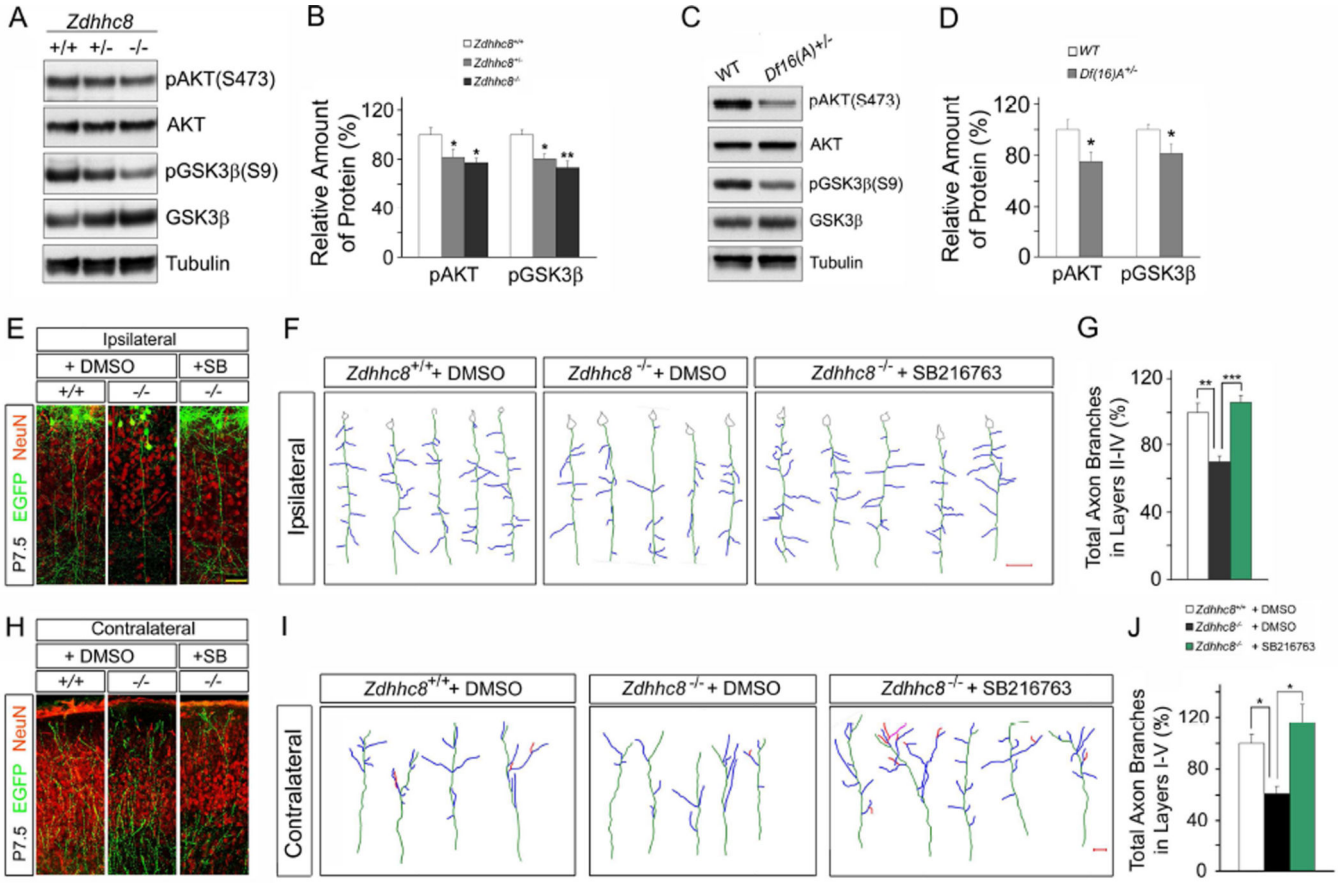

Figure 8. SB216763 treatment restores axon branch numbers

(**A, B**) Western blot analysis of lysates of prefrontal cortex from *Zdhhc8*-deficient mice at 8 weeks demonstrating reduced levels of pAKT(S473) and pGSK3β(S9).

(**C, D**)Western blot analysis of lysates of prefrontal cortex from *Df16(A)*$^{+/-}$ mice at 8 weeks demonstrating reduced levels of pAKT(S473) and pGSK3β(S9).

(**E**) Representative images of ipsilateral axon branching of EGFP–labeled neurons from coronal sections of SB216763-treated brain at P7.5.

(**F**) Traces of axon branches in the ipsilateral cortical layers 2–4 of coronal sections from P7.5 brains *in utero* electroporated with EGFP at E15.5 and treated with DMSO or SB216763 from P2 to P7.

(**G**) Quantification of axon morphology reveals that SB216763 treatment restored axon branch numbers in the ipsilateral cortical layers 2–4. Scale bar, 20 μm.

(**H**) Representative images of contralateral axon branching of EGFP–labeled neurons from coronal sections of SB216763-treated brain at P7.5.

(**I**) Traces of axon branches in the contralateral cortical layers 2–4 of coronal sections from P7.5 brains *in utero* electroporated with EGFP at E15.5 and treated with DMSO or SB216763 from P2 to P7.

(**J**) Quantification of axon morphology reveals that SB216763 treatment restored axon branch numbers in the contralateral cortical layers 1–4. Scale bar, 20 μm.

Data are shown as means ± s.e.m. *, $P < 0.05$; **, $P < 0.001$; ***, $P < 0.0001$; Student's t-test.